ORTA DOĞU TEKNİK ÜNİVERSİTESİ
FEN BİLİMLERİ ENSTİTÜSÜ MÜDÜRLÜĞÜ

TEZ ŞABLONU ONAY FORMU
THESIS TEMPLATE CONFIRMATION FORM

1. Şablonda verilen yerleşim ve boşluklar değiştirilmemelidir.

2. Jüri tarihi Başlık Sayfası, İmza Sayfası, Abstract ve Öz'de ilgili yerlere yazılmalıdır.

3. İmza sayfasında jüri üyelerinin unvanları doğru olarak yazılmalıdır.

4. Tezin son sayfasının sayfa numarası Abstract ve Öz'de ilgili yerlere yazılmalıdır.

5. Bütün chapterlar, referanslar, ekler ve CV sağ sayfada başlamalıdır. Bunun için **kesmeler** kullanılmıştır. **Kesmelerin kayması** fazladan boş sayfaların oluşmasına sebep olabilir. Bu gibi durumlarda paragraf (¶) işaretine tıklayarak kesmeleri görünür hale getirin ve yerlerini **kontrol edin**.

6. Figürler ve tablolar kenar boşluklarına taşmamalıdır.

7. Şablonda yorum olarak eklenen uyarılar dikkatle okunmalı ve uygulanmalıdır.

8. Tez yazdırılmadan önce PDF olarak kaydedilmelidir. Şablonda yorum olarak eklenen uyarılar PDF dokümanında yer almamalıdır.

9. Bu form aracılığıyla oluşturulan PDF dosyası arkalı-önlü baskı alınarak tek bir spiralli cilt haline getirilmelidir.

10. Spiralli hale getirilen tez taslağınızdaki ilgili alanları imzalandıktan sonra, Tez Juri Atama Formu ile birlikte bölüm sekreterliğine teslim edilmelidir.

11. Tez taslağınız bölüm sekreterliğiniz aracılığıyla format ve görünüm açısından kontrol edilmek üzere FBE'ye ulaştırılacaktır.

12. FBE tarafından kontrol işlemleri tamamlanan tez taslakları, öğrencilere teslim edilmek üzere bölüm sekreterliklerine iletilecektir.

13. Tez taslaklarının kontrol işlemleri tamamlandığında, bu durum öğrencilere METU uzantılı öğrenci e-posta adresleri aracılığıyla duyurulacaktır.

14. Tez taslakları bölüm sekreterlikleri tarafından öğrencilere iletileceği için öğrencilerimizin tez taslaklarını enstitümüzden elden alma konusunda ısrarcı olmamaları beklenmektedir.

15. Tez yazım süreci ile ilgili herhangi bir sıkıntı yaşarsanız, **Sıkça Sorulan Sorular (SSS)** sayfamızı ziyaret ederek yaşadığınız sıkıntıyla ilgili bir çözüm bulabilirsiniz.

1. Do not change the spacing and placement in the template.

2. Write defense date to the related places given on Title page, Approval page, Abstract and Öz.

3. Write the titles of the examining committee members correctly on Approval Page.

4. Write the page number of the last page in the related places given on Abstract and Öz pages.

5. All chapters, references, appendices and CV must be started on the right page. **Section Breaks** were used for this. **Change in the placement** of section breaks can result in extra blank pages. In such cases, make the section breaks visible by clicking paragraph (¶) mark and **check their position.**

6. All figures and tables must be given inside the page. Nothing must appear in the margins.

7. All the warnings given on the comments section through the thesis template must be read and applied.

8. Save your thesis as pdf and Disable all the comments before taking the printout.

9. Print two-sided the PDF file that you have created through this form and make a single spiral bound.

10. Once you have signed the relevant fields in your thesis draft that you spiraled, submit it to the department secretary together with your Thesis Jury Assignment Form.

11. Your thesis draft will be delivered to the GSNAS via your department secretary for controlling in terms of format and appearance.

12. The thesis drafts that are controlled by GSNAS, will be sent to the department secretary to be delivered to the students.

13. This will be announced to the students via their METU students e-mail addresses when the control of the thesis drafts has been completed.

14. As the thesis drafts will be delivered to the students by the department secretaries, we are expecting from our students no to insist about getting their theses drafts from the Institute.

15. If you have any problems with the thesis writing process, you may visit our **Frequently Asked Questions (FAQ)** page and find a solution to your problem.

☒ **Yukarıda bulunan tüm maddeleri okudum, anladım ve kabul ediyorum. / I have read, understand and accept all of the items above.**

Name : Üçel
Surname : Kaan
E-Mail : e233930@metu.edu.tr
Date : 09.05.2022
Signature : ________________________

DESIGN OF A DUAL POLARIZED LOW PROFILE ANTENNA FOR MICROWAVE BRAIN IMAGING

A THESIS SUBMITTED TO
THE GRADUATE SCHOOL OF NATURAL AND APPLIED SCIENCES
OF
MIDDLE EAST TECHNICAL UNIVERSITY

BY

KAAN ÜÇEL

IN PARTIAL FULFILLMENT OF THE REQUIREMENTS
FOR
THE DEGREE OF MASTER OF SCIENCE
IN
ELECTRICAL AND ELECTRONICS ENGINEERING

MAY 2022

Approval of the thesis:

DESIGN OF A DUAL POLARIZED LOW PROFILE ANTENNA FOR MICROWAVE BRAIN IMAGING

submitted by **KAAN ÜÇEL** in partial fulfillment of the requirements for the degree of **Master of Science in Electrical and Electronics Engineering Department, Middle East Technical University** by,

Prof. Dr. Halil Kalipçilar
Dean, Graduate School of **Natural and Applied Sciences** ________________

Prof. Dr. İlkay Ulusoy
Head of Department, **Electrical and Electronics Engineering** ________________

Assoc. Prof. Dr. Lale Alatan
Supervisor, **Electrical and Electronics Engineering, METU** ________________

Examining Committee Members:

Prof. Dr. Gülbin Dural
Electrical and Electronics Engineering, METU ________________

Assoc. Prof. Dr. Lale Alatan
Electrical and Electronics Engineering, METU ________________

Prof. Dr. Özlem Aydin Çivi
Electrical and Electronics Engineering, METU ________________

Assist. Prof. Dr. Ahmet Cemal Durgun
Electrical and Electronics Engineering, METU ________________

Prof. Dr. Birsen Saka Tanatar
Electrical and Electronics Engineering, Hacettepe University ________________

Date: 09.05.2022

I hereby declare that all information in this document has been obtained and presented in accordance with academic rules and ethical conduct. I also declare that, as required by these rules and conduct, I have fully cited and referenced all material and results that are not original to this work.

Name, Surname : Kaan ÜÇEL

Signature :

ABSTRACT

DESIGN OF A DUAL POLARIZED LOW PROFILE ANTENNA FOR MICROWAVE BRAIN IMAGING

Üçel, Kaan
M.Sc, Electrical and Electronics Engineering
Supervisor: Assoc. Prof. Dr. Lale Alatan

May 2022, 52 pages

In this thesis, a low profile, low cost, wide band (0.9-2GHz) dual linearly polarized printed dipole antenna is designed to be used in microwave brain imaging systems. Dual polarization feature offers superior data acquisition through polarization diversity for better image quality. Starting from a simple printed dipole, antenna structure is modified step by step to meet these design requirements. Since a conductive surface in close vicinity of the antenna affects antenna performance, in order to obtain unidirectional radiation from the dipole, instead of an electric conductor, a frequency selective surface (FSS) surface is utilized to obtain a low profile antenna. The designed antenna has 11x11x1.8 cm dimensions. The antenna is manufactured on a FR-4 substrate by laser etching machine. Return loss performance and radiation pattern characteristics are measured in an anechoic chamber. Measurement and simulation results have been compared with each other and satisfactory relevance is achieved.

Keywords: Printed Dipole, Wideband Antennas, Dual Polarized Antenna

ÖZ

MİKRODALGA BEYİN GÖRÜNTÜLEME İÇİN ÇİFT POLARİZE DÜŞÜK PROFİLLİ ANTEN TASARIMI

Üçel, Kaan
Yüksek Lisans, Elektrik Elektronik Mühendisliği Bölümü
Tez Danışmanı: Doç. Dr. Lale Alatan

Mayıs 2022, 52 sayfa

Bu tezde, mikrodalga beyin görüntüleme sistemlerinde kullanılmak üzere düşük profilli, düşük maliyetli, geniş bantlı (0.9-2GHz) doğrusal çift polarize baskılı dipol anten tasarlanmıştır. Çift polarizasyon özelliği, daha iyi görüntü kalitesi için polarizasyon çeşitliliği yoluyla üstün veri toplama becerisi sunar. Basit bir basılı dipolden başlayarak, bahsedilen tasarım gereksinimlerini karşılamak için anten yapısı adım adım geliştirilmiştir. Antenin yakınında bulunan iletken bir yüzey anten performansını etkilediğinden, dipolden tek yönlü radyasyon elde etmek için iletken bir yüzey yerine frekans seçici yüzey (FSS) yüzeyi kullanılarak düşük profilli bir anten elde edilmiştir. Tasarlanan anten 11x11x1.8 cm boyutlarındadır. Anten, lazer kazıma makinesi ile FR-4 substratı üzerine üretilmiştir. Geri dönüş kaybı performansı ve radyasyon modeli özellikleri, yankısız bir odada ölçülür. Ölçüm ve simülasyon sonuçları birbiriyle karşılaştırılarak tatmin edici bir uygunluk elde edilmiştir.

Anahtar Kelimeler: Basılı Dipol, Geniş Bantlı Antenler, Çift Polarize Anten

To my loving family

ACKNOWLEDGMENTS

I would like to express my very gratitude and appreciation to my supervisor Assoc. Prof. Dr. Lale Alatan for her patience, guidance and support from the start of this study.

I would like to thank my family for their love and support during harder times of preparing this thesis.

I would like to thank Melek for her unending love and support during preparation of this thesis.

I would like to thank my colleague, Erkan Çankaya for his indulgence and understanding that helped me find time to study during busy work schedules.

I would like to thank İlkay Karataş for invaluable assistance during antenna measurements.

I would like to thank my friends for their continuous support and entertainment to burn as fuel to complete this thesis.

TABLE OF CONTENTS

ABSTRACT v
ÖZ vi
ACKNOWLEDGMENTS viii
TABLE OF CONTENTS ix
LIST OF TABLES x
LIST OF FIGURES xi
LIST OF ABBREVIATIONS xiii
CHAPTERS
Introduction 1
Antenna Design 7
2.1. Initial Model 7
2.2. Systematic Examination of Antenna Parameters 11
2.3. Increasing the Bandwidth of the Dipole 14
2.4. Radiation Pattern 20
2.5. Frequency Selective Surface 26
2.5. Near Field Analysis with Head Phantom 35
Measurement Results 41
3.1. Realized Antenna 41
3.2. Antenna Measurements 43
Conclusion and Future Work 48
4.1. Conclusion 48
4.2. Future Work 49
References 51

LIST OF TABLES

Table 1. Relation between dipole length vs longest operatinonal wavelength............................ 14

LIST OF FIGURES

FIGURES

Figure 1. Abbosh's low-cost and small monopole antenna [15] 4
Figure 2. Mobashsher's folded dipole antenna (a)Top view (b)Side view [19] 4
Figure 3. Deng's dual polarized patch antenna [21] 5
Figure 4. Mobashsher and Abbosh's microwave imaging system [22] 6
Figure 5. Initial model 8
Figure 6. Current distribution on initial model at a) 800MHz b)1364MHz 10
Figure 7. Asymmetric radiation due to unequal feeding of dipole arms 10
Figure 8. Return loss performance of initial model 10
Figure 9. Dimensions of the antenna 11
Figure 10. Effect of gap width between dipole arms on antenna performance 12
Figure 11. Effect of substrate thickness on antenna s11 performance 13
Figure 12. Effect of antenna length on s11 performance of the antenna 13
Figure 13. Model with tapered arms 15
Figure 14. Return loss performance of tapered model 15
Figure 15. Partially tapered model 16
Figure 16. Return loss performance of three different dipole structures 17
Figure 17. Return loss performance of partially tapered model for various r2 values 18
Figure 18. Model with extensions on each dipole arm 18
Figure 19. Surface currents behavior around extension 19
Figure 20. Parameters of extension 19
Figure 21. Return loss performance of extended model for various parameter values 20
Figure 22. Orientation of the antenna 21
Figure 23. Radiation patterns on E and H planes for various models and frequencies 22
Figure 24. Surface current distributions for taperless and partially tapered models 23
Figure 25. Surface current distributions for tapered model 24
Figure 26. Co-pol and cross-pol radiation patterns on E-plane for various models and frequencies 26
Figure 27. Radiation pattern of partially tapered model on E-plane 27
Figure 28. Partially tapered model with perfect electric conductor (reflector) 27
Figure 29. Radiation pattern of partially tapered model with reflector and no reflector cases on E-plane 28
Figure 30. Effect of reflector distance on s11 performance 29

Figure 31. FSS unit cell model and simulation setup 30
Figure 32. Reflection and Transmission performance of FSS unit cell 31
Figure 33. Reflection phase of FSS unit cell 31
Figure 34. Antenna with FSS configuration 32
Figure 35. s11 performance of antenna with FSS 33
Figure 36. Radiation pattern of antenna with and without FSS @1GHz 34
Figure 37. Co-pol E Field Radiation Patterns on E-Plane for various models and frequencies .. 34
Figure 38. Simulation configuration with human head model 35
Figure 39. Effect of introducing head model on s11 performance 36
Figure 40. Interaction between horizontally oriented antennas for various configurations 36
Figure 41. Interaction between vertically oriented antennas for various configurations 37
Figure 42. Interaction between antennas without head model for various configurations 38
Figure 43. Interaction between antennas with head model for various configurations 38
Figure 44. Coupling between antennas on the same substrate for various configurations 39
Figure 45. Electric field distribution at 1GHz, 1.4GHz, 1.8GHz 40
Figure 46. Electric field distribution with FSS and without FSS 40
Figure 47. Top view of the realized antenna 41
Figure 48. Top view of realized frequency selective surface 42
Figure 49. Manufactured antenna and FSS 42
Figure 50. Simulated vs measured s11 results 43
Figure 51. Simulated vs measured s21 results 44
Figure 52. Anechoic chamber and measurement setup 44
Figure 53. Measured vs simulated co-pol radiation patterns in E-plane for various FSS distances and frequencies 46
Figure 54. Measured vs simulated co-pol and crosspol radiation patterns in E-plane for various frequencies 47
Figure 55. Measured vs simulated co-pol radiation patterns in H-plane for various frequencies 47
Figure 56. Flexible antenna with PDMS substrate 50

LIST OF ABBREVIATIONS

PEC	Perfect Electric Conductor
PMC	Perfect Magnetic Conductor
FSS	Frequency Selective Surface
PDMS	poly-di-methyl-siloxane
RF	Radio Frequency

CHAPTER I

Introduction

For the last decade, there has been an increased interest in rapid, on-site diagnosis techniques. For this reason, microwave imaging became a popular topic for building low cost, portable medical tools to be used especially in remote areas. There are various studies for imaging different body parts [1], [2]. Head is one of the most important areas since medical traumas concerning brain tend to deteriorate more swiftly if it is not diagnosed rapidly. Due to portability requirements, on-site microwave imaging tools must be small and relatively simple which limits the imaging capability of the system. Instead of constructing high quality images, these systems detect the difference in electrical properties between healthy and unhealthy areas in the brain. Detection quality is closely related to the amount of data gathered from the head. There are several image reconstruction techniques [3], [4], [4], [5], [6] proposed to obtain the image from the gathered data. Antenna is one of the most important elements in the system since it determines the amount and diversity (i.e., different frequencies, polarizations) of collected data.

Most microwave imaging systems consists of multiple antennas that work with multiple input multiple output (MIMO) principle. In a MIMO system, one antenna transmits at a time and the data received by all other antennas are recorded. Particularly for head imaging, antennas are placed around the head forming a helmet-like structure [1]. These antennas gather scattered field from the target area to be used in image reconstruction algorithms. Increasing the number of antennas results in an improvement in image quality. Since the system size is limited, only way of increasing the number of antennas is reducing the antenna size. There have been many studies [1], [7], [8], [10], [11] on the miniaturization of antennas for microwave imaging. This thesis introduces a small, dual polarized, wideband antenna to be used in a portable microwave imaging system. The benefit of having a wide frequency band is that resolution in the image improves with increasing bandwidth [6]. Moreover, when a tissue is illuminated with different frequencies, different reflection or scattering mechanisms occur. Consequently, the scattered field data at various frequencies provide more information about the electrical properties of the target. Similarly, more information about scattering from the imaging space can be obtained by utilizing dual polarization. In addition to that, as stated by Huygen's principle if tangential components of electric and magnetic fields are known over a closed surface, fields outside and inside that surface can be found. Hence when the field is sampled on the hemispherical surface with dual polarization, it provides tangential component. Consequently, a better image quality is expected. The challenge of introducing dual polarization is that it usually requires two antennas with separate feeds which contradicts with small antenna size requirement.

Unlike traditional medical imaging systems, microwave imaging systems can be used in areas which are susceptible to high traffic of wireless signals. However, since the target area is the head which is within the enclosed helmet-like structure, antennas must be receiving signals only from head. Otherwise, unwanted signals coming from outside the system can degrade the imaging quality. Therefore, low back lobe levels and high front to back ratio is required. Such requirements can be met by using directional antennas or by adding reflective or directive elements to the system. Problem with reflective and directive elements is that when placed in close proximity to the antenna, they can alter matching performance of the antenna and make design of the main radiating antenna element much harder. Also, if they are not placed close to the antenna these elements increase the system size significantly. For this reason, in recent years periodic structures like frequency selective surfaces (FSS) or resistive impedance substrates (RIS) started to be widely used instead of electric conductors [12].

Although medical microwave imaging is still not a commonly available technique, its foundations go as early as 1970s. Electromagnetic waves can damage tissues by heating even if it is a nonionizing wave. For this reason, early studies about microwave imaging focus on effects of EM waves on human body and proper illumination strength. In 1972, Michaelson documented effects of various wavelengths on organs and protection guides [13]. Again in 1972, Johnson proposed a microwave imaging instrument on cat's head along with a study on penetration and absorption characteristics of several frequencies on brain [14]. According to these studies 918 and 2450 MHz are the optimum frequency limits for penetration and absorption, respectively. Later studies suggest similar frequency bands for microwave imaging [15], [16]. Idea behind the optimum frequency is that lower frequencies have more penetration through tissues. Since different parts of the brain have different permittivity, waves go through some tissues while absorbed by other tissues. This mechanism is used to locate various parts in the brain. If frequency is too low, wave goes through all tissues and no tissue is detected. Same problem is valid for high frequencies since if wave is completely absorbed, no data can be obtained. Therefore, using a band of frequencies to be scattered in brain enables the system to identify various tissues. On the other hand, power of waves must be below a specific level to avoid heating of the tissues. This challenge can be easily overcame by modern receivers with high sensitivity that enable illumination power for microwave imaging systems to be remarkably below safety limits.

Yamaura introduced another microwave imaging system in 1977 employing horn antennas for 1.8-2.7 GHz frequency band, further investigating the dynamics of illuminating human torso and receiving scattered signals [17]. In his work, he focuses on leakage effects and coupling between antenna and human body. Compared to modern microwave imaging systems, Yamaura's system was very basic mainly because of low received signal quality and processing capabilities. With increasing processing power, advanced numerical methods are developed for solving inverse scattering problem. In 1991, Joachimowicz introduced an iterative method for microwave tomography approach which created a basis for advanced image reconstruction algorithms [18]. Further developments have shown benefits of using multiple frequencies and employing multiple antennas simultaneously [16]. However multiple antenna approach introduces physical size problem especially for portable systems.

In 2006, Abbosh introduced a low loss, ultra-wide band (3-12GHz) printed monopole antenna for microwave imaging as shown in Figure 1 [15]. One downside of this antenna was its omnidirectional radiation pattern, making the system susceptible to background noise. Nevertheless, such an easy to manufacture, relatively small antenna enabled low-cost, portable microwave imaging systems.

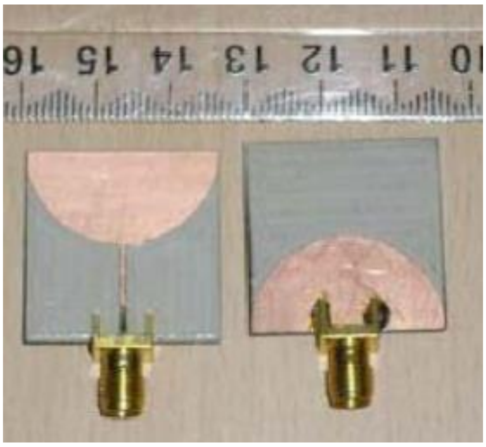

Figure 1. Abbosh's low-cost and small monopole antenna [15]

Since then, numerous antennas are developed for microwave imaging [19], [20], [21], [21], [23], [23], [24], [25]. Each of these antennas focus on one or several aspects of the microwave imaging requirements while compromising on other properties. For example, Figure 2 shows the antenna Mobashsher proposed in 2013 [19] which achieves operating frequency band of 1-3GHz, directional radiation pattern and low profile while compromising on lowest operating frequency which determines penetration capacity. The miniaturized version of the same antenna [20] offers half size while compromising on the bandwidth (1.25-2.4GHz).

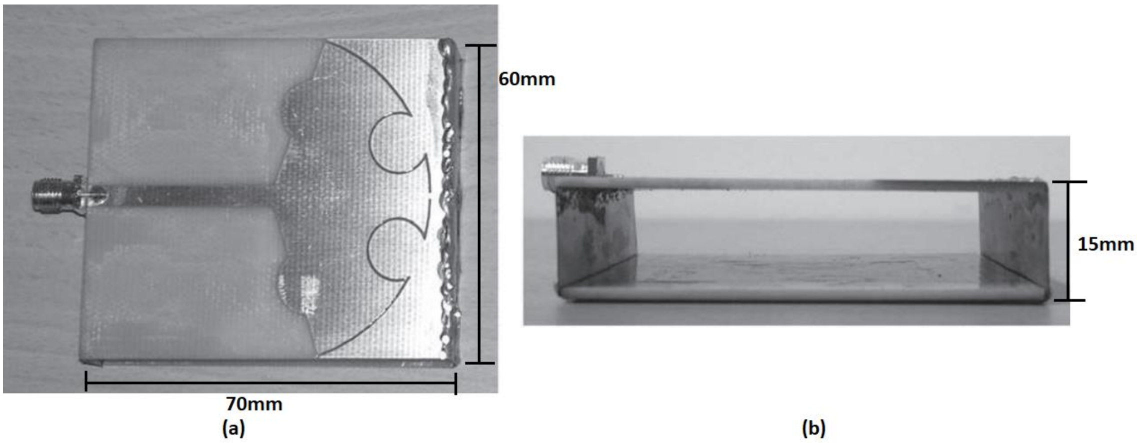

Figure 2. Mobashsher's folded dipole antenna (a)Top view (b)Side view [19]

Deng proposed an antenna in 2014 [21] which offers dual polarization at the cost of size (60x60mm radiating element, 100x100x10mm with feeding network and the reflector) and bandwidth (2.2-2.6GHz). As shown in Figure 3, dual polarization is obtained by integrating a printed dipole antenna with a bowtie shaped slot antenna. Since dual polarization usually requires two separate antennas or similar structure with separate feedings, keeping antenna size low is a design challenge for dual polarized antennas. In this thesis, the requirement on the size of the antenna is eased to achieve dual polarization operation.

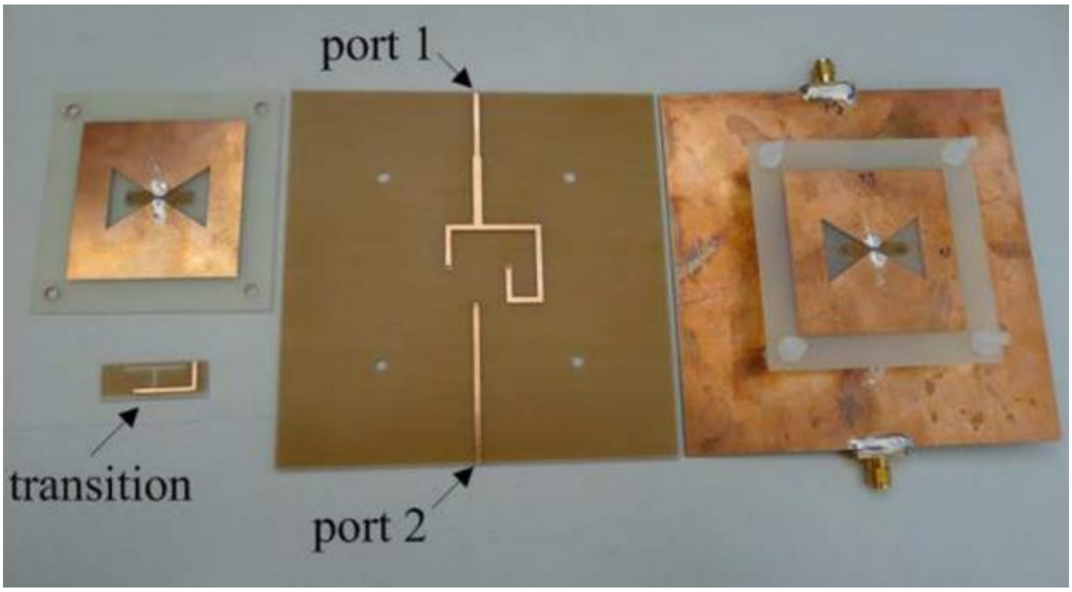

Figure 3. Deng's dual polarized patch antenna [21]

In 2016, Mobashsher and Abbosh introduced another antenna for microwave imaging of brain and incorporated it into a helmet-like system [21]. The system also has a switching circuitry and a transceiver behind the antennas. Figure 4 shows the antenna used in this system which is a 10x10x80mm slot-loaded folded dipole with 1-2.4GHz operating frequency band and 3dBi average gain. In this thesis, an antenna with similar performance is proposed with added feature of dual polarization.

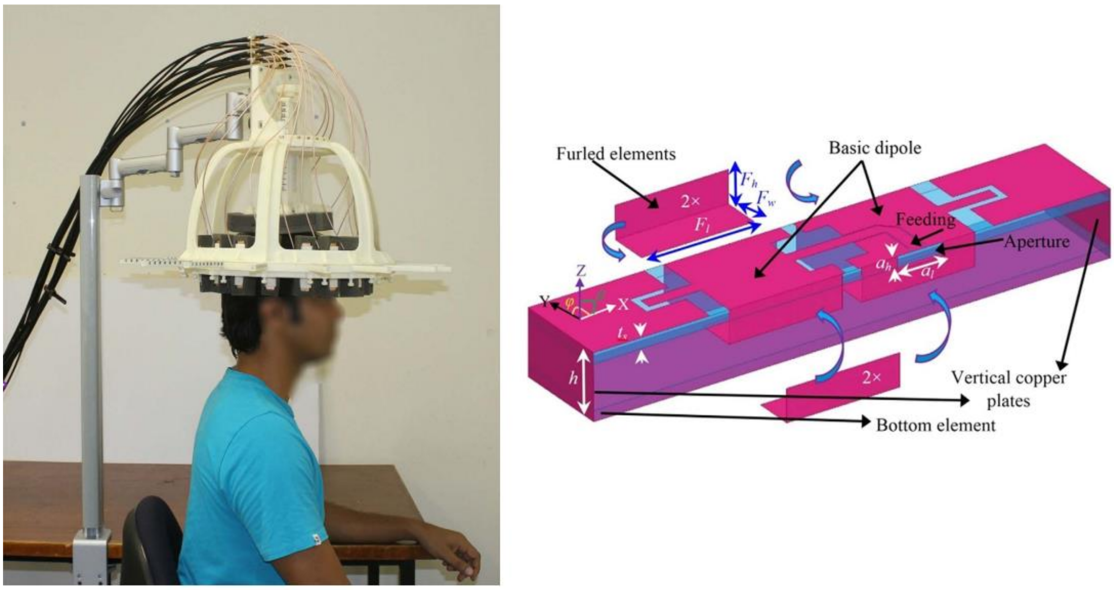

Figure 4. Mobashsher and Abbosh's microwave imaging system [21]

The thesis consists of 4 main chapters. In this introduction chapter, historical development of microwave imaging for the head along with recent developments on antennas proposed for such systems is described.

In the second chapter, design process of the proposed antenna is presented step by step starting with a simple printed dipole and ending with the final form of the antenna. Simulations ran on CST Studio Suite 2019 examined and results discussed. Design considerations between each step and discussions on simulation results are given. Along with return loss performance, radiation pattern characteristics are also discussed. Benefits and working mechanism of various added features of the antenna are explained. In the last section, detailed simulation results and realistic configurations using a human head model are investigated.

In the third chapter, measurement results of the manufactured antenna are investigated. Scattering parameters and radiation pattern results are compared to simulation results.

In the fourth chapter, possible further developments on this particular antenna and in microwave imaging in general are discussed. Design and obtained results are summarized.

CHAPTER II

Antenna Design

2.1. Initial Model

For microwave imaging of brain, using low profile antennas enable the imaging system to be simple and mobile. Microstrip technology provides such compact and cost-efficient antennas in the form of printed antennas. In this work, a pair of printed dipole antennas are integrated to gather dual polarized information. Two separate orthogonal linearly polarized antenna configuration is referred as dual polarized antenna. Each antenna is excited independently and data from both polarization components can be processed separately. Starting with a pair of simple printed dipoles, a more complex version is obtained.

Since brain has many layers with different dielectric properties, antenna must operate on a wide frequency band to penetrate, reflect or scatter from these mediums so that different layers can be distinguished and a useful image can be constructed. Researches show 900MHz is enough for penetrating all layers of the brain [13]. Therefore, starting operating frequency band from 900MHz is optimal for maximum penetration capability. On the other hand, when frequency is too high losses inside the brain increases and less scattered signal is received. Therefore 2.45GHz is chosen as desired upper limit [13]. Figure 5 shows the initial model which is a simple dual polarized antipodal printed dipole antenna. The antenna dimensions are 11x11cm and is printed on a FR-4 substrate with 1.5 mm thickness. The term antipodal refers to a structure where instead of placing 2 arms of a dipole on the same side of the substrate, they are placed on opposite sides. In Figure 5 green color refers to conductors on one side and pink color refers to the conductors on other side. There are several examples of such configuration used in antenna miniaturization [1], [19], [20]. This way one of the arms of the dipole acts as the ground of microstrip feedline. This makes feeding the antenna very easy and simple without needing a hole through the substrate or a balun to feed the dipole arms. Antipodal design also increases isolation between dipole pairs, thus improving cross-polarization performance which is one of the main concerns for a dual-polarized design.

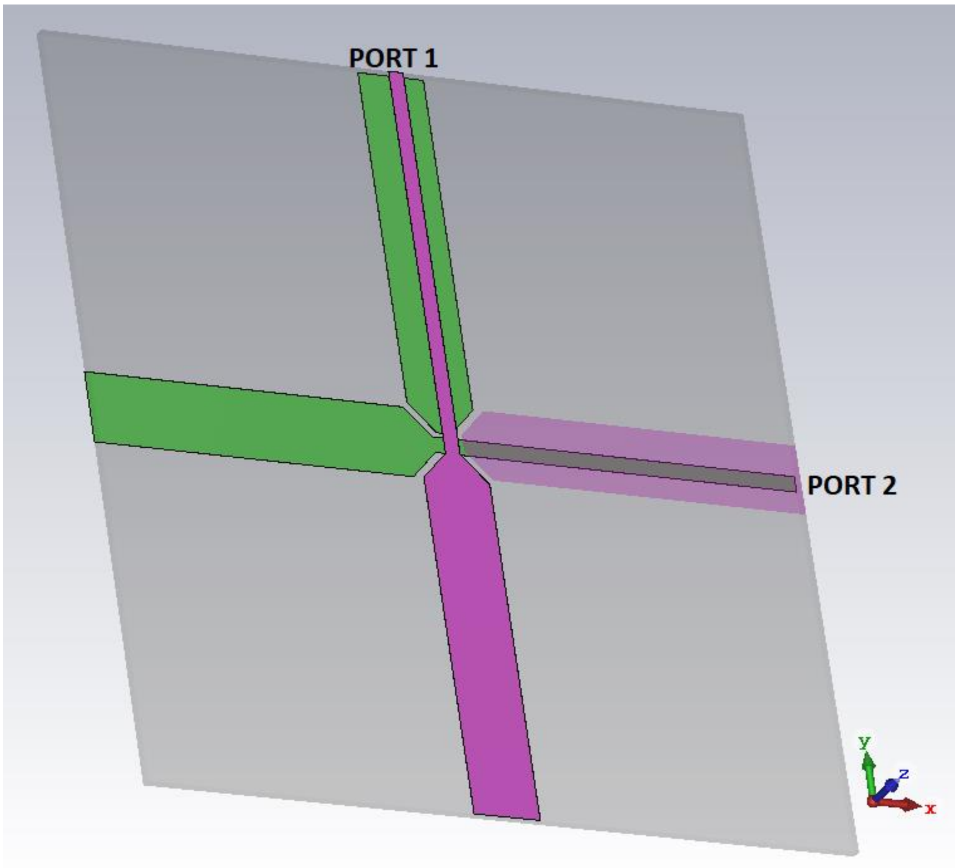

Figure 5. Initial model

We can examine the surface current distribution to understand the working principle of both the feeding technique and the dipole itself. Figure 6 shows the current distribution on dipole arms at 800MHz and 1364MHz. Top arm is in lower side of the substrate while feedline and bottom arm are on the upper side of the substrate. When fed from the port on the top, currents flow downwards on the microstrip line and feeds the bottom dipole arm in downwards directions at 800 MHz. Top arm of dipole serves as the ground plane for the microstrip line. Therefore, currents flow towards the port on top arm in the region just below the feedline. On the other hand, at the edges of the top arm, current flows in the same direction as the bottom arm. As it can be observed from the radiation pattern plots provided in Figure 7, the opposite directed currents on the feed line and the region below the feedline cancel each other and the edge currents on the top arm and the currents on the bottom arm results in the expected dipole pattern. When current distributions at 1.364 GHz are examined it can be observed that they are in same direction for top and bottom arms but it is stronger at the top arm. As a result, due to unequal feeding of dipole arms, an asymmetry is observed in the radiation pattern as seen in Figure 7. The reason for such a change in the current distribution is the change in the electrical length of the feed line with frequency. At 1.364 GHz the feed line is almost quarter of the wavelength whereas it is about 0.15 wavelength at 800 MHz. With the change in the electrical length, the impedance seen at the excitation port changes and this affects the variation of current along the feedline both in magnitude and phase. Later in this thesis, we will further investigate surface current distribution for upcoming models.

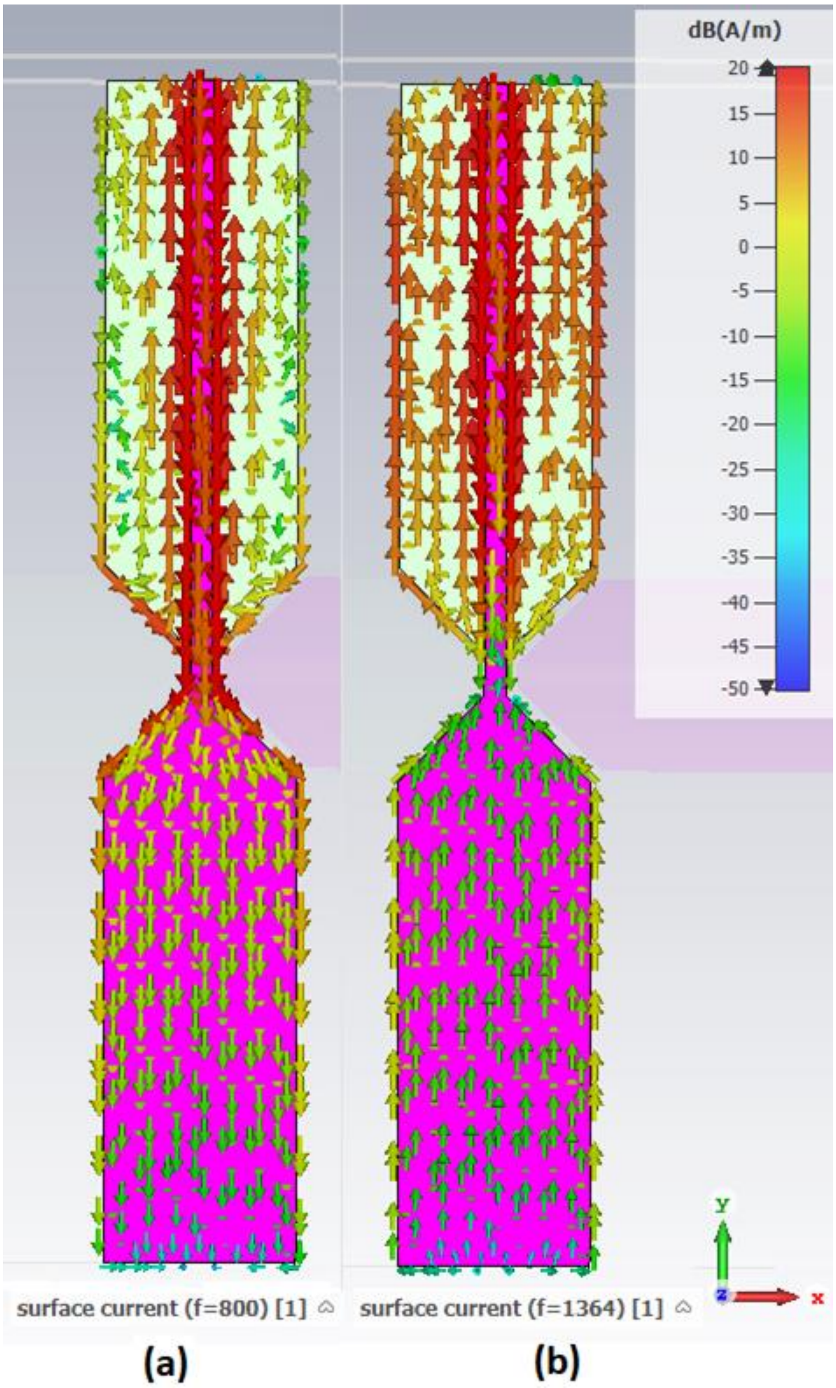

Figure 6. Current distribution on initial model at a) 800MHz b)1364MHz

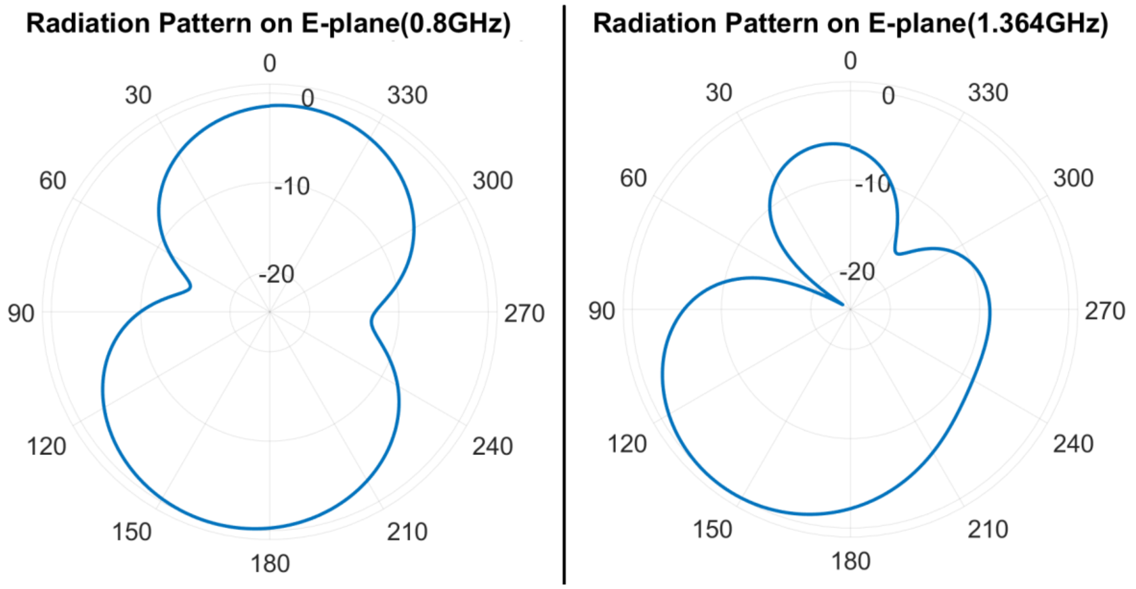

Figure 7. Asymmetric radiation due to unequal feeding of dipole arms

Figure 8 shows the return loss at feeding port of the antenna. -10dB return loss is usually considered as minimum acceptable performance and we will refer to "operating frequency band" as frequencies where return loss is lower than -10dB. For the initial model, frequency bandwidth is about 200MHz around 800MHz center frequency. Our aim is to achieve an operating band from 900 MHz to 2GHz for maximum penetration capability.

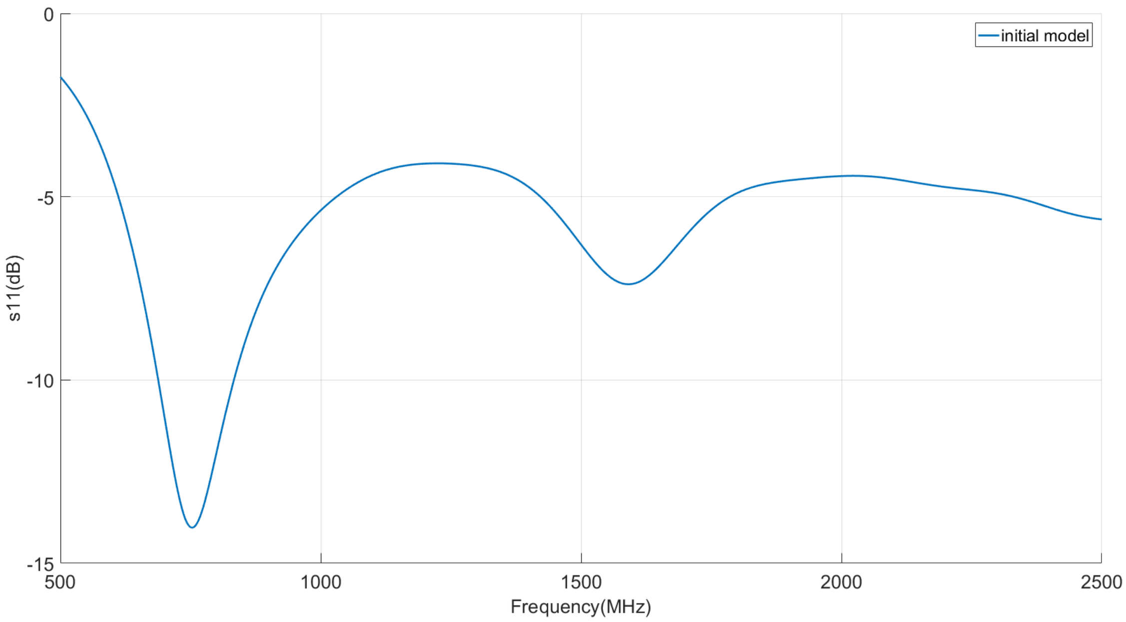

Figure 8. Return loss performance of initial model

2.2. Systematic Examination of Antenna Parameters

There are several parameters defining the overall performance of the antenna. Each of these parameters affects the performance of the antenna in a specific way. These effects must be studied systematically to understand the radiation mechanism and to optimize the antenna performance. Each dimension must be isolated and effect of small changes of these dimensions on overall performance needs to be observed independently. Main parameters are antenna length, space between dipole arms and substrate thickness. Figure 9 shows these dimensions and corresponding parameters for these dimensions on the proposed antenna. For the initial model, these parameters are chosen as gapc=4mm, feedw=2mm, Ldip=110mm, Wdip=3mm.

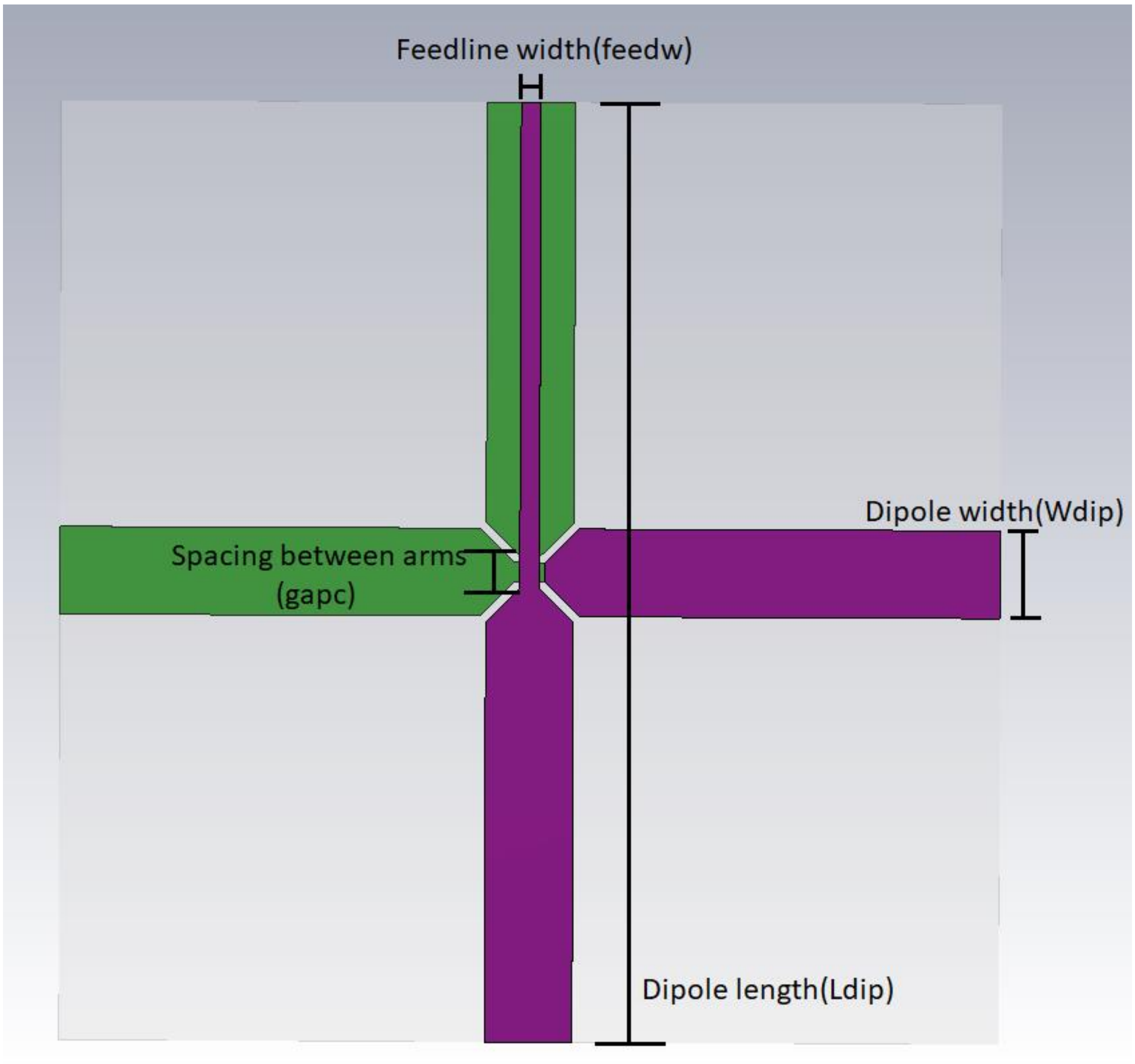

Figure 9. Dimensions of the antenna

Although two printed dipoles are fed independently, since they are on the same substrate and close to each other, both affect each other's radiation mechanism. This effect is closely related to isolation between two orthogonally polarized antennas which determines the cross-polarization performance of the antenna. Suppressed cross-polarization allows proper separation of the information obtained from different polarization components, resulting in better image reconstruction. Increasing the distance between antennas increases the isolation and improves overall antenna performance. Figure 10 shows the effect of distance between dipole arms on the antenna performance. Increasing this distance improves bandwidth slightly and reduces s_{11} values considerably for the whole band. This may be due to the change in the capacitance value of the gap between the dipole arms. Hence this parameter of the antenna can be used to improve the matching of the antenna.

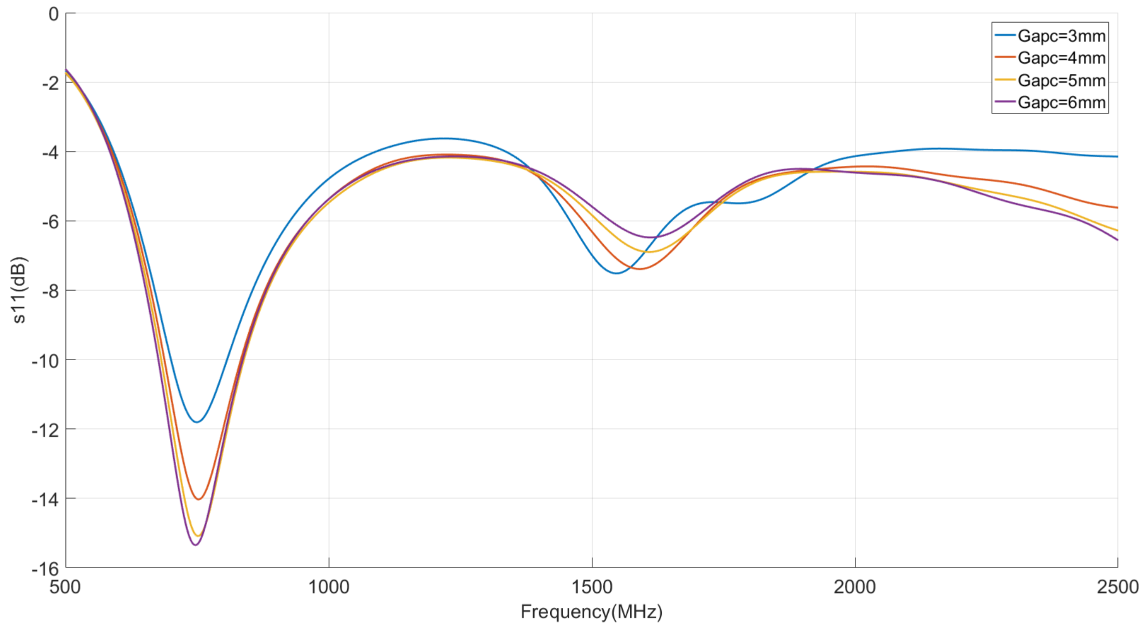

Figure 10. Effect of gap width between dipole arms on antenna performance

Thickness of the antenna substrate also affects the antenna performance. Since substrate thickness is determined by the materials used in manufacturing, not every desired thickness is available. Figure 11 shows the effect of substrate thickness on s_{11} performance of the antenna. Increasing the substrate thickness slightly improves s_{11} performance. This effect may also be due to the change in capacitance values of the gap between dipole arms. Similarly, this parameter can also be tuned for better matching.

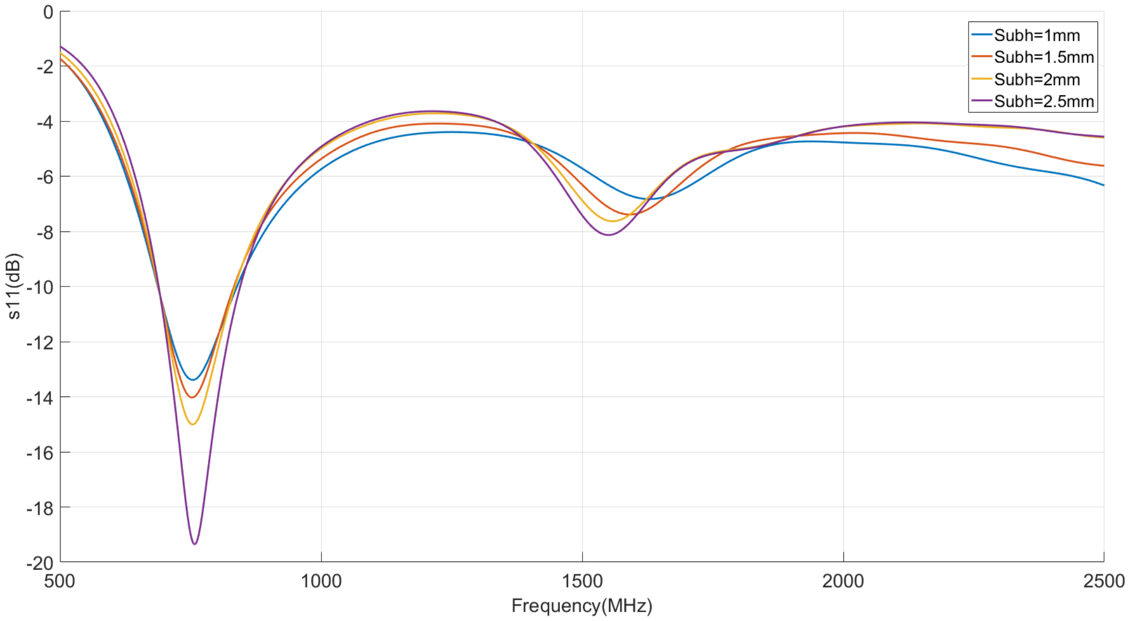

Figure 11. Effect of substrate thickness on antenna s_{11} performance

Antenna length is the primary dimension determining the frequency of operation. Figure 12 shows the effect of antenna length on the s_{11} performance of the antenna. As expected, increasing antenna length shifts the operational bandwidth to lower frequencies.

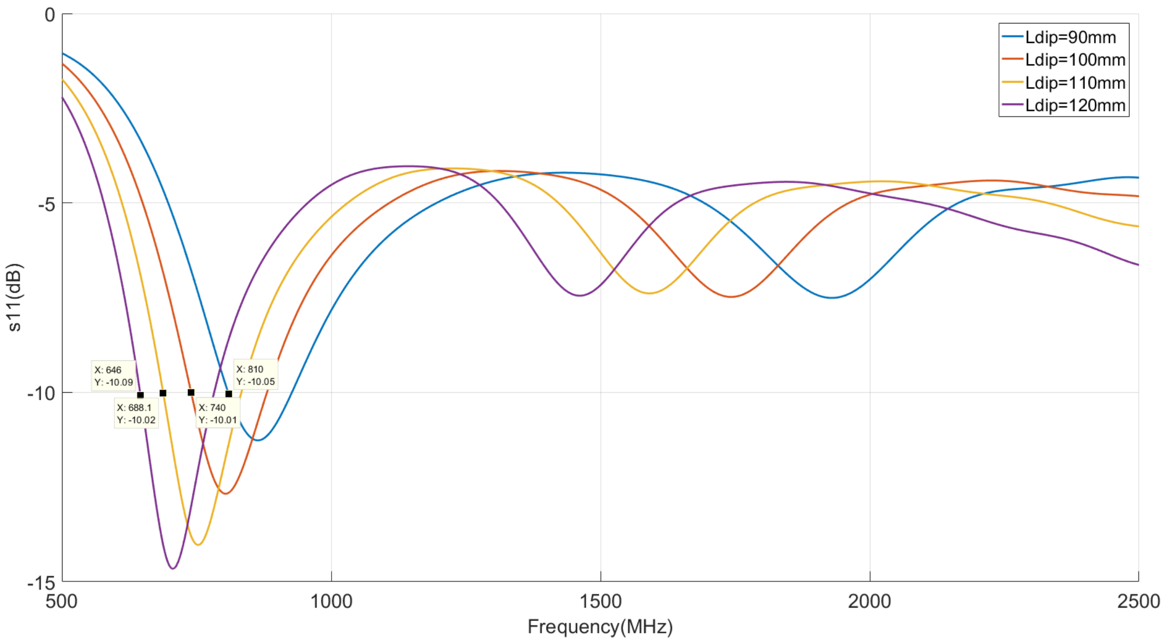

Figure 12. Effect of antenna length on s_{11} performance of the antenna

Table 1 shows the relation between dipole length and longest wavelength supported by the corresponding dipole length. L_{dip}/λ_{low} ratio is approximately 0.25 for all lengths, suggesting that lower frequency cut-off occurs when dipole length is quarter wavelength. Note that another resonance occurs when dipole length corresponds to half wavelength. However, the matching level at that frequency is not as good as the matching at the lower band. Hence, the aim will be to improve matching at the higher resonance and in between two resonances to achieve wider bandwidth.

Table 1. Relation between dipole length vs longest operatinonal wavelength

L_{dip} (mm)	f_{low} (MHz)	λ_{low} (mm)	L_{dip}/λ_{low}
90	**810**	**370**	**0.24**
100	**740**	**405**	**0.25**
110	**688**	**436**	**0.25**
120	**646**	**464**	**0.26**

Since it is well known that the width of the dipole significantly affects the bandwidth, its effects will be analyzed separately in the next section.

2.3. Increasing the Bandwidth of the Dipole

As discussed in Introduction chapter, wider frequency band provides better image quality. Therefore, improvements on the simple printed dipole must be made. A common way to achieve this is to employ tapered arms instead of fixed width along the arm length as shown in Figure 13. Tapering allows the spreading of the current along the width of the antenna. This spreading of the current reduces the variation of the current distribution with changing frequency. Consequently, bandwidth gets wider. Tapered structure also makes maximum use of the antenna area. Figure 13 shows the design with tapered dipole arms.

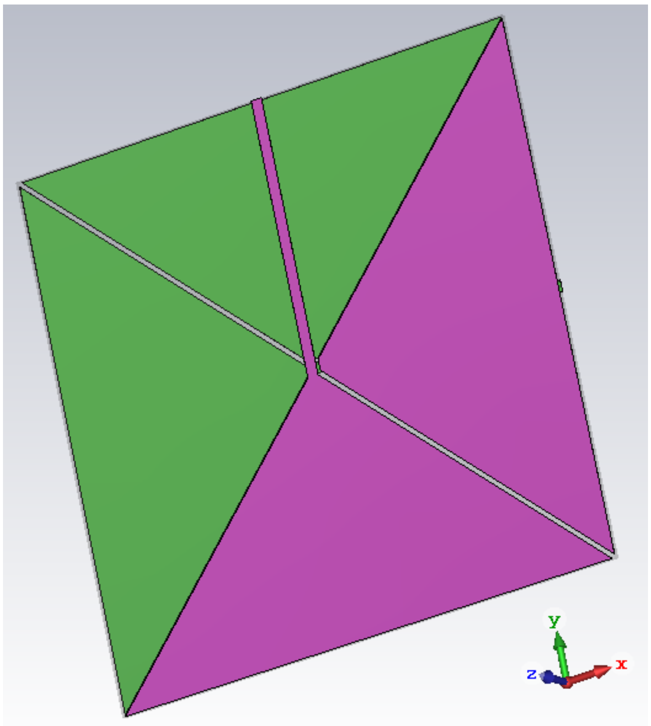

Figure 13. Model with tapered arms

Figure 14 shows the return loss performance of tapered model and confirms the mentioned mechanism above. Bandwidth is increased from 200MHz to almost 500MHz while the bandwidth shifted towards higher frequencies. Since the frequency band starts from about 900MHz after this shift, the antenna still meets the requirements on lower frequency limit.

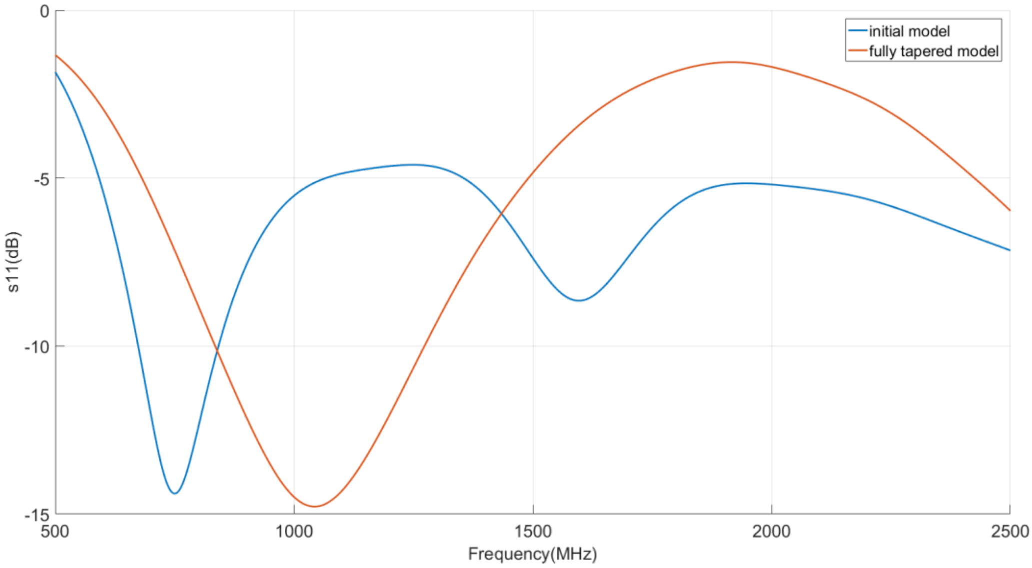

Figure 14. Return loss performance of tapered model

Based on the geometries of wideband printed dipole antenna structures in literature, a partially tapered model as shown in Figure 15 is also investigated.

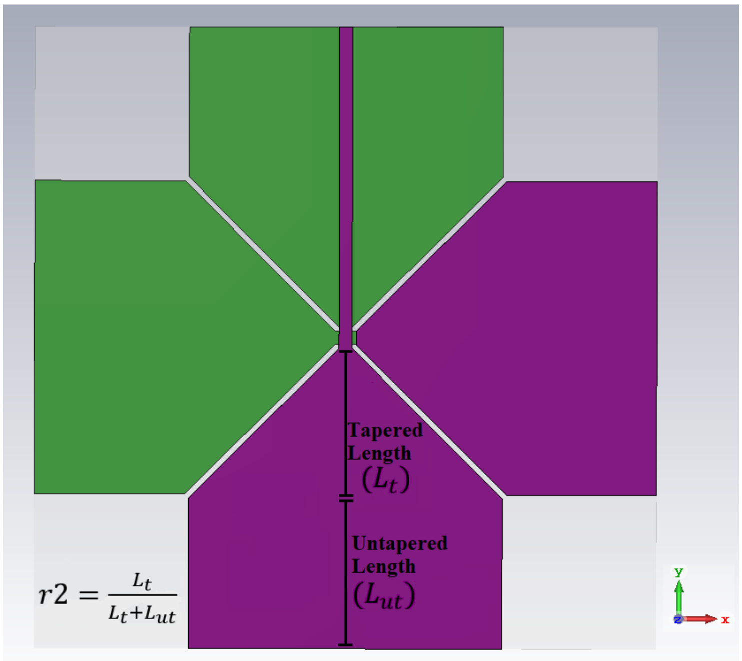

Figure 15. Partially tapered model

Figure 16 shows the return loss performance of the partially tapered model compared to previous models. Bandwidth is further increased to nearly 1.5GHz, while keeping the lower frequency limit almost same as the narrow dipole antenna. Another interesting observation is that the matching level at the second resonance frequency (around 1.6GHz) of the narrow dipole is improved significantly by making the width of the dipole wider.

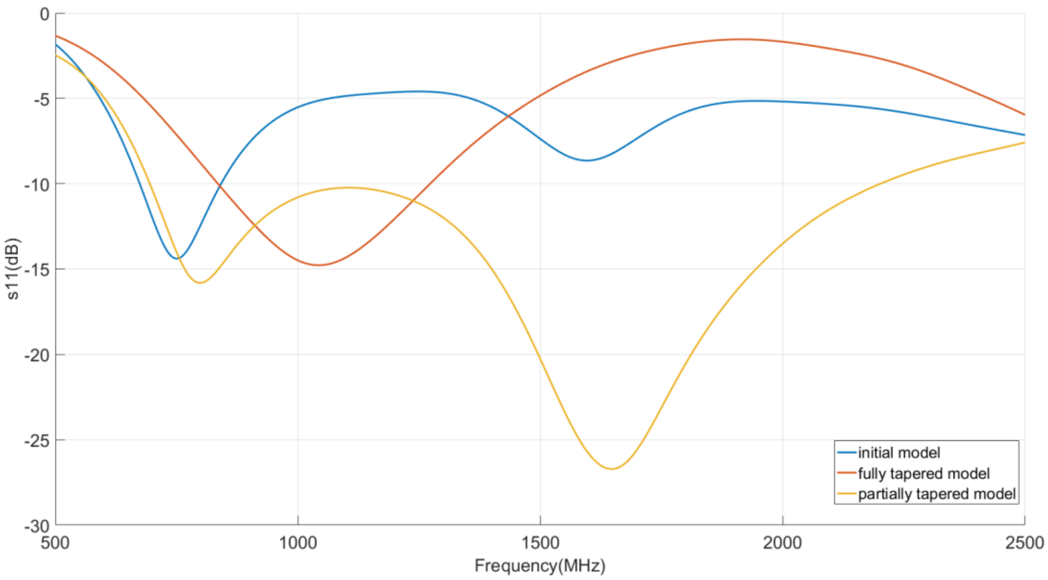

Figure 16. Return loss performance of three different dipole structures

This large bandwidth is achieved by sweeping r2 which is the ratio of the length of the tapered portion of the dipole arm to the entire dipole arm length as shown in Figure 15. Note that as this ratio increases, the width of the untapered portion of the dipole gets wider. When ratio is 1, it is equivalent to fully tapered model and when ratio is 0.15, it corresponds to initial model. Figure 17 shows return loss performance of the partially tapered dipole model for various r2 values. It is shown that bandwidth as wide as 1.5GHz around 1.4GHz can be achieved when r2 is chosen as 0.35. Note that increasing the ratio improves the return loss value at two resonances until r2=0.35. With further increase in the ratio, the resonance at higher frequency disappears, lower frequency cut-off increases, two resonances merge into one and bandwidth gets narrower.

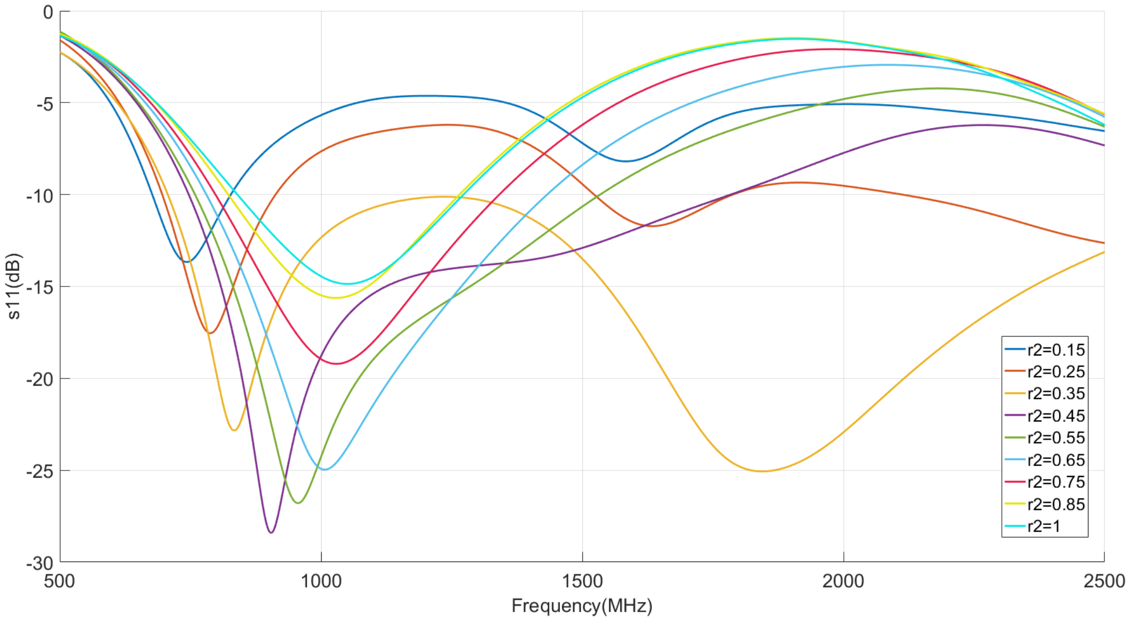

Figure 17. Return loss performance of partially tapered model for various r2 values

Although desired antenna performance can be achieved with the tapered model, 11cm antenna length limits the number of antennas in the system. If effective dipole length can be kept constant while decreasing the overall antenna size, a smaller antenna can be obtained for similar operating frequency band. To increase the effective dipole length, the dipole arms are extended towards both sides as shown in Figure 18.

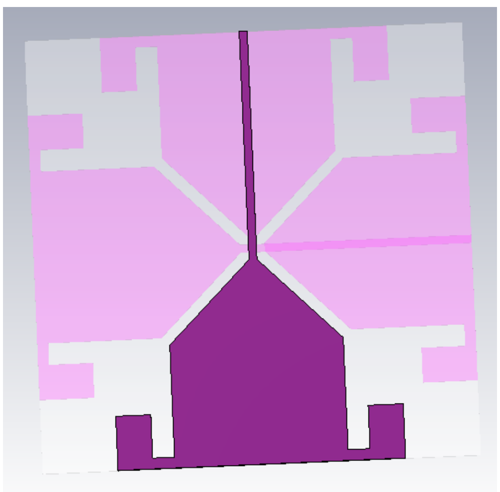

Figure 18. Model with extensions on each dipole arm

Although extended current paths are expected to lower minimum operating frequency to our benefit, this addition will definitely alter s_{11} performance as well as radiation properties since currents on different directions are introduced. Figure 19 shows such current distribution around the extension.

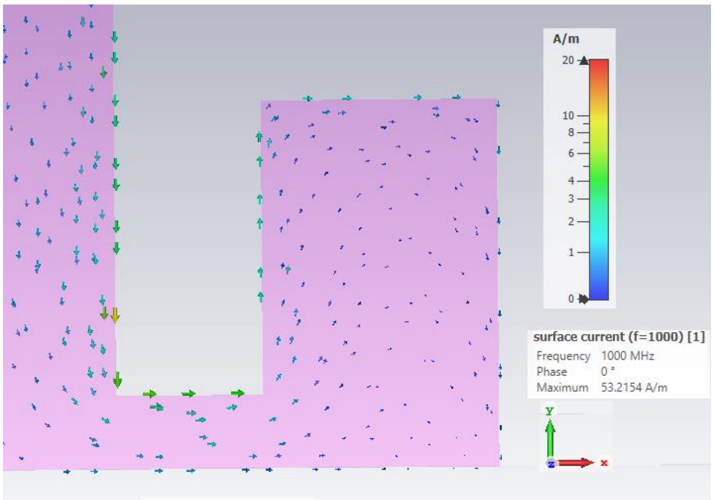

Figure 19. Surface currents behavior around extension

Also, as spacing between dipole pairs decrease, coupling between dipole pairs increase, worsening isolation between ports. Figure 20 shows the description of design parameters on an extension.

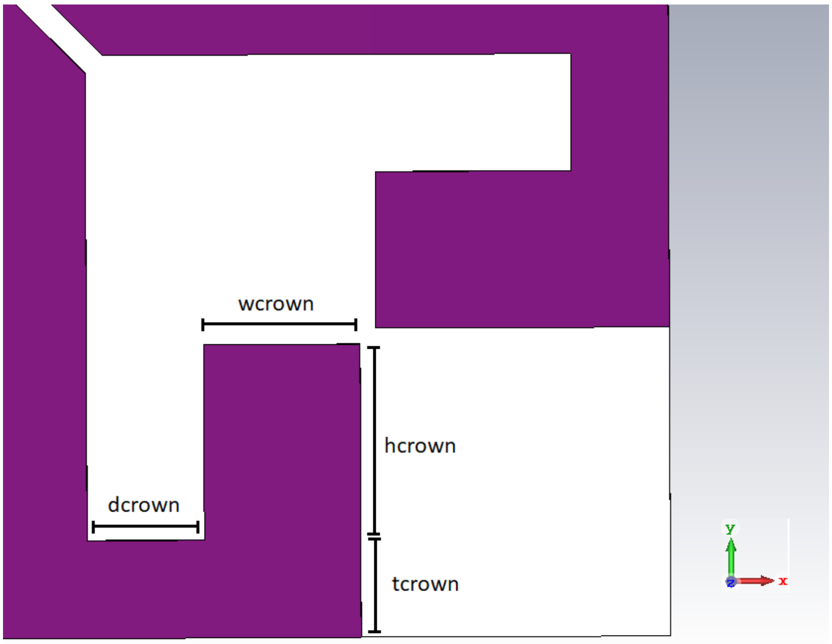

Figure 20. Parameters of extension

Effect of each extension dimension is studied. For parametric sweep, parameters are in terms of ratio to the dipole length. Figure 21 shows the s_{11} performance of extended model for various values of extension dimensions.

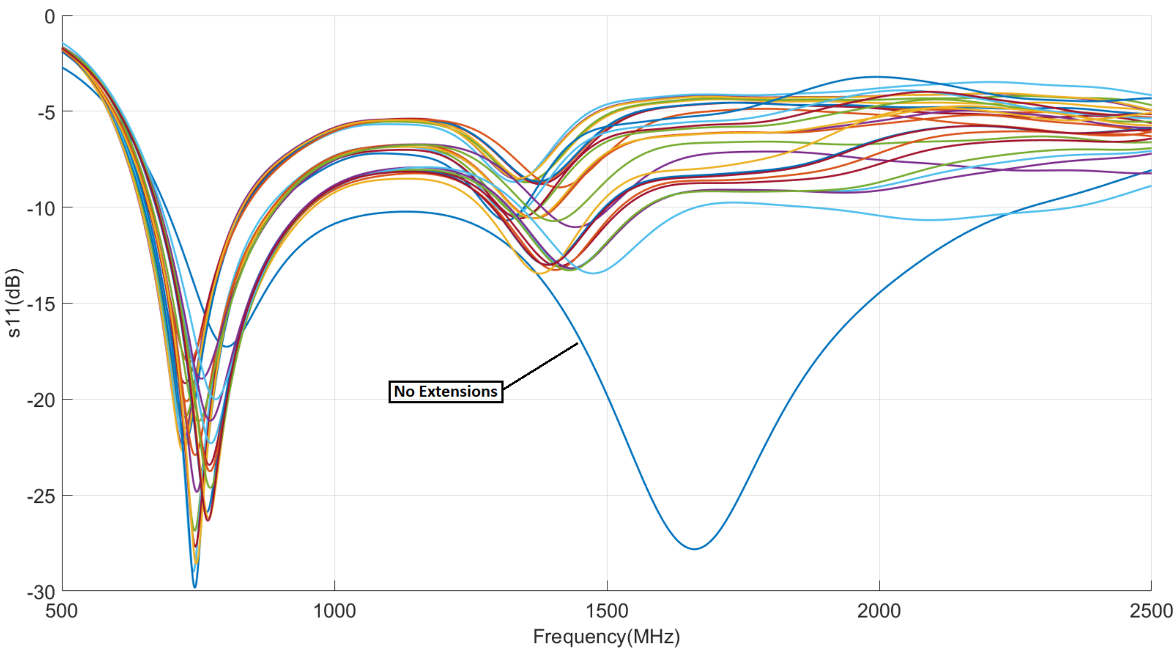

Figure 21. Return loss performance of extended model for various parameter values

Lowest operating frequency is slightly decreased since currents have longer paths. Therefore, antenna size can be reduced compared to design without extensions to achieve same operating frequency band. However, bandwidth is reduced greatly which is not a reasonable trade-off. Hence, partially tapered model is chosen as the final design instead of extended model. Final antenna parameters are Ldip=110mm, subh=1.5mm, r2=0.35, gapc=4mm, feedw=2.5mm. Copper thickness is 18µm.

2.4. Radiation Pattern

Although return loss is an important parameter for determining operating frequency band, radiation pattern must be examined as well to validate performance of the antenna. Figure 22 shows the orientation of the antenna and angle definitions.

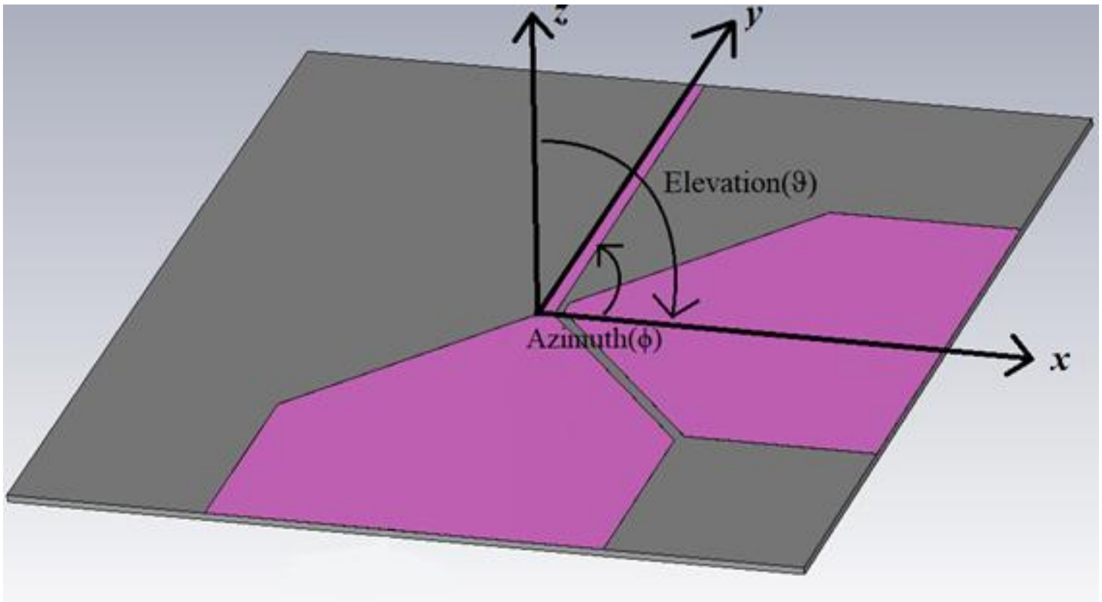

Figure 22. Orientation of the antenna

Typically, the radiation patterns are plotted in 2D slices through the 3D pattern for simplification. Figure 23 shows radiation patterns on E and H planes for various antenna models and frequencies. It is worth noting that these patterns are normalized individually. This makes examining front to back ratios and lobe shapes easier. They could be normalized to a constant maximum for all results for comparison. It is clear that partially tapered model exhibits almost omnidirectional radiation in H-plane for all frequencies. Such radiation is typical for dipole antennas. On the other hand, in E-plane, dipole antenna is expected to radiate with equal magnitude and beamwidth towards front and back side with nulls on side directions. Although magnitude is similar for front and back directions, it is clear that partially tapered model exhibits asymmetric radiation especially in terms of beam shape.

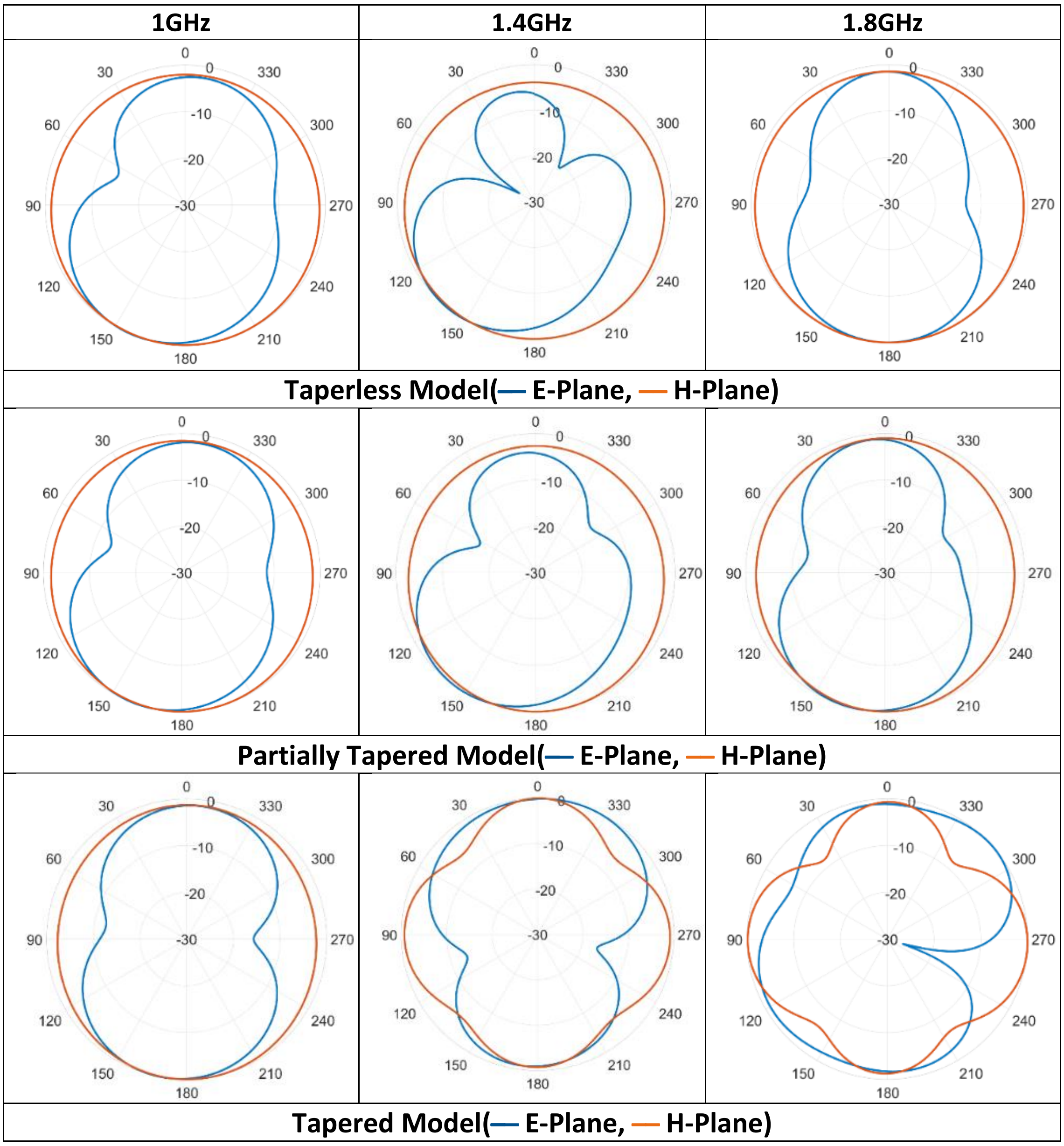

Figure 23. Radiation patterns on E and H planes for various models and frequencies

To understand the reason for asymmetries in E-plane patterns, current distributions for different antenna models at different frequencies are presented in Figure 24 and Figure 25. Although it is more convenient to feed the antenna with the proposed mechanism from a practical standpoint, as mentioned in previous sections, dipole arms cannot be fed equally for all frequencies in operating band. Figure 24 confirms such mechanism since although currents flow in same direction on both dipole arms for all frequencies, there are differences in magnitude. It can be observed that asymmetries in both radiation patterns and surface current distributions occur when two dipole arms are not excited equally.

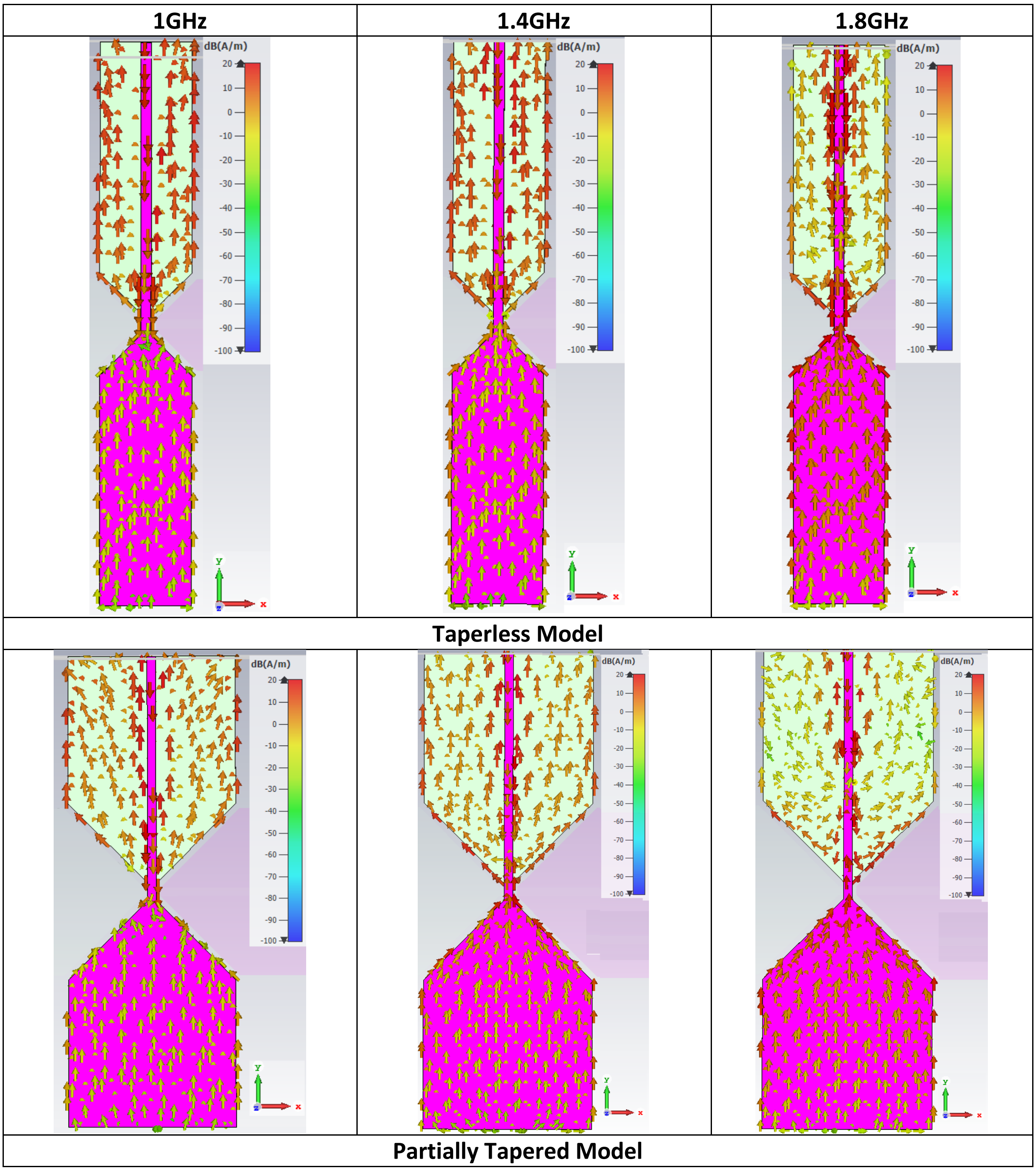

Figure 24. Surface current distributions for taperless and partially tapered models

Tapered Model @1GHz	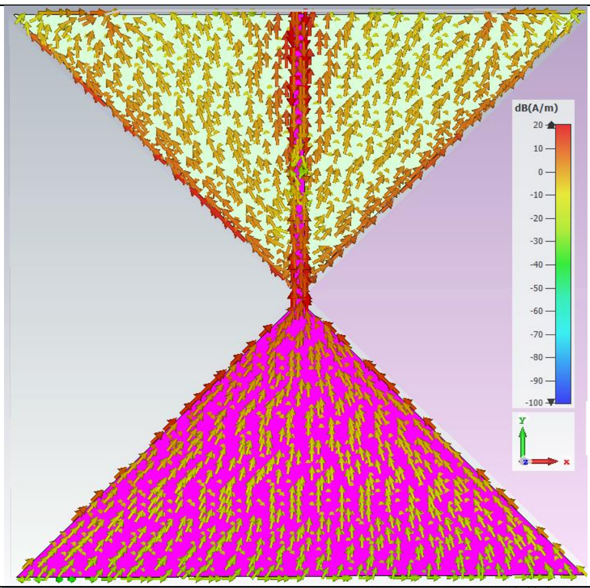
Tapered Model @1.4GHz	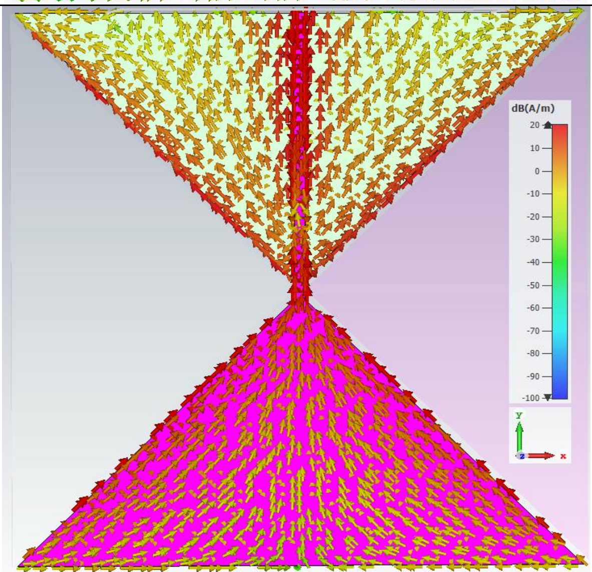
Tapered Model @1.8GHz	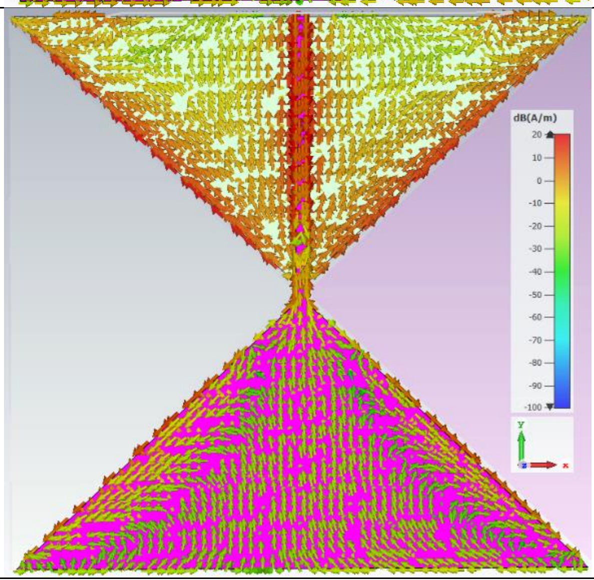

Figure 25. Surface current distributions for tapered model

Since dual polarization is one of the main features of the proposed antenna, cross-polarization performance must also be investigated. Suppressed cross-polarization allows data obtained from orthogonal polarization components to be separated. Figure 26 shows co-pol and cross-pol radiation patterns on E-plane for various frequencies and antenna models.

As it can be observed from current distribution plots, when dipole arms are tapered, surface currents spread, which may lead to higher cross-pol levels. Figure 26 confirms such mechanism since as we go from taperless model to tapered model, cross-pol radiation increases. While cross-pol level relative to co-pol level is -50dB for taperless model at 1GHz, it is -35dB for partially tapered model and -30dB for tapered model. It is worth noting that cross-pol radiation also increases for higher frequencies. While cross-pol level for partially tapered model is -35dB for 1GHz, it is -30dB for 1.4GHz and -25dB for 1.8GHz. This might be due to the fact that the width of the dipole becomes electrically larger with increasing frequency and consequently current spread increases.

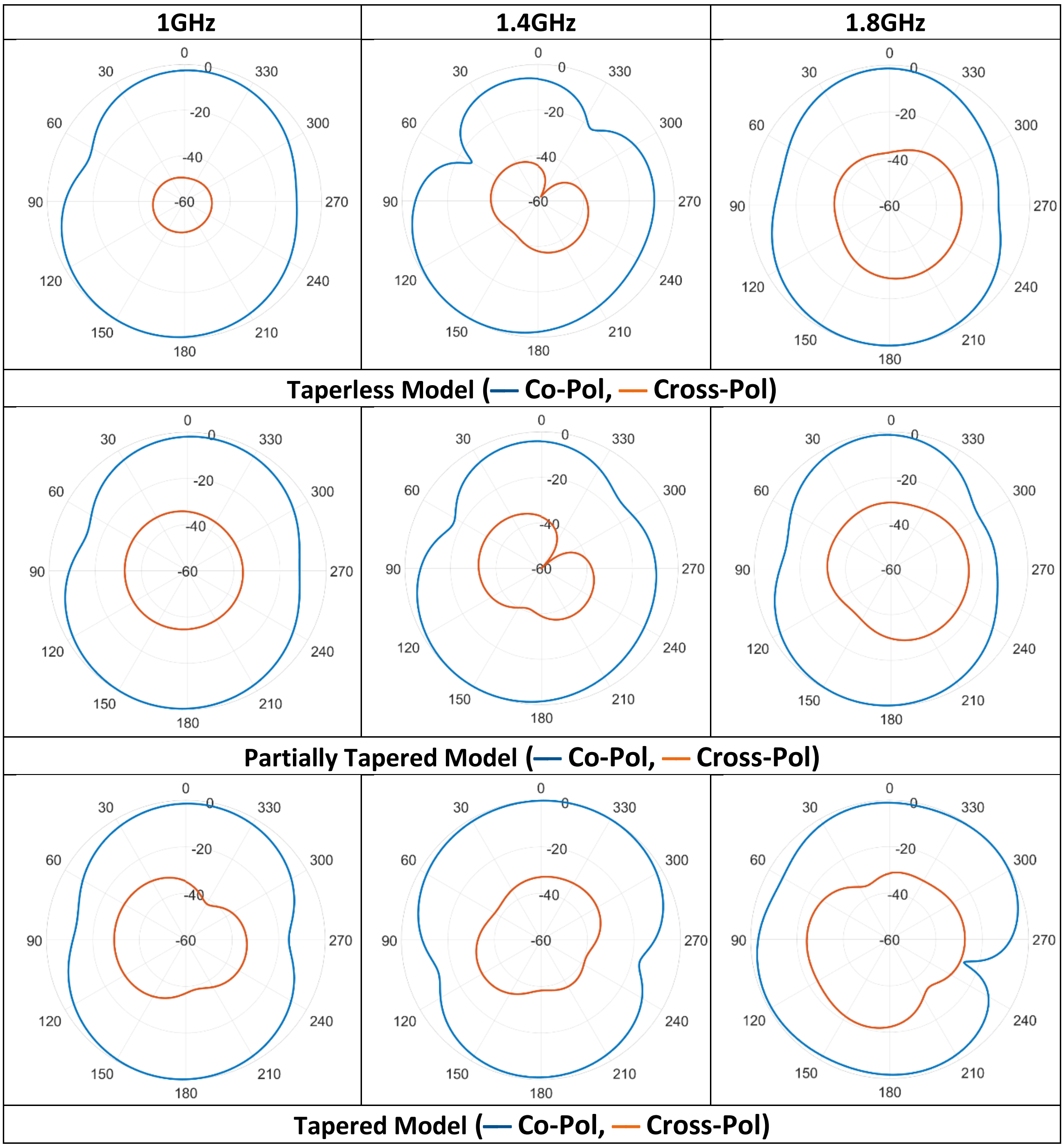

Figure 26. Co-pol and cross-pol radiation patterns on E-plane for various models and frequencies

2.5. Frequency Selective Surface

Radiation characteristics of the partially tapered model can be modified in order to meet the system requirements. Figure 27 shows the radiation pattern of partially tapered model on E-plane. Such radiation pattern is typical for dipole antennas and indicates that antenna is radiating towards front and back side almost equally. However, since the target area to be imaged is going to be only on front side, power received from the back side will increase the received noise power. Therefore, we need to minimize back side radiation.

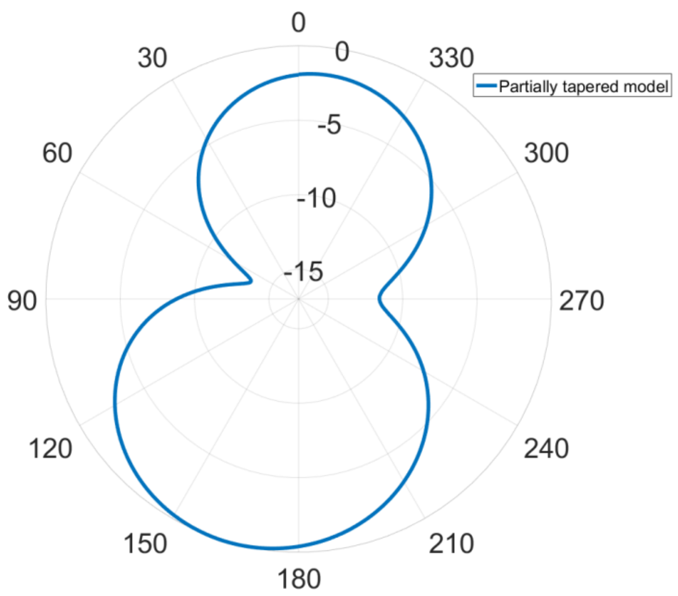

Figure 27. Radiation pattern of partially tapered model on E-plane

Since low front to back ratio is inherent for dipole antennas, any modification on the radiating element itself wouldn't help achieving our goal. Increasing front to back ratio can be achieved by placing a reflecting or absorbing surface behind the antenna. Figure 28 shows the partially tapered model with a perfect electric conductor (PEC) of the same size (green colored in the figure) placed behind the antenna.

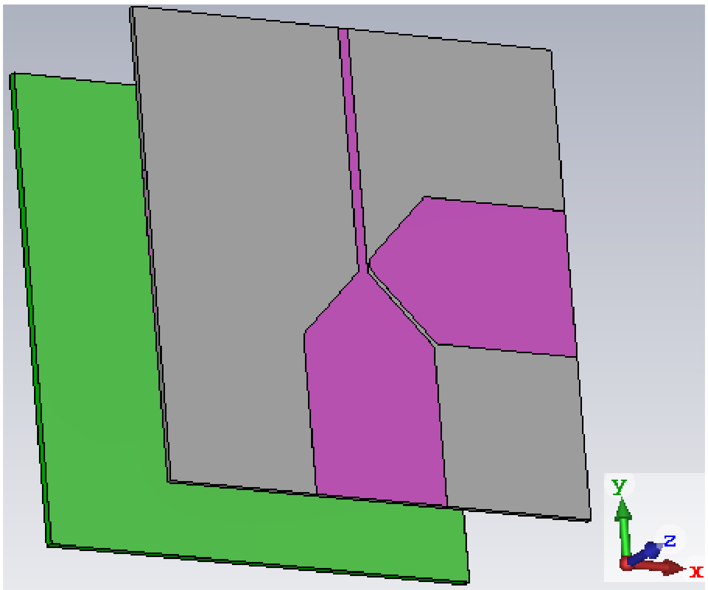

Figure 28. Partially tapered model with perfect electric conductor (reflector)

The conductor sheet behind the antenna reflects waves coming from back side, reducing noise coming from the environment while increasing the signal power radiated into target area. However, since we introduce a conductor in near field of the antenna, it affects the input impedance of the antenna. It must be placed at a specific distance from the antenna to avoid performance degradation. Figure 29 shows the radiation pattern on E-plane when conductor is placed 1.5cm behind the antenna. Back side radiation is reduced by 9dB. Still, return loss performance must be examined to ensure wide bandwidth. Figure 30 shows effect of distance between conductor (reflector) and the antenna (refdist) on s_{11} performance. To get a decent bandwidth for the current radiating element, at least 15cm space between antenna and reflector is needed. This means height of the antenna increases at least 15cm. This is practically unacceptable since helmet-like structure gets too bulky for a portable system.

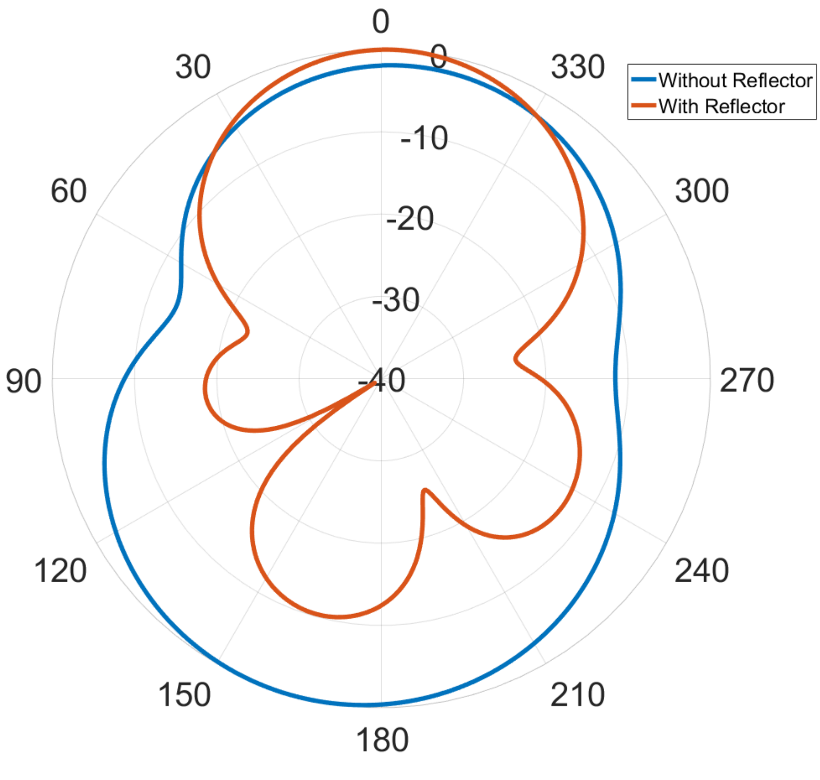

Figure 29. Radiation pattern of partially tapered model with reflector and no reflector cases on E-plane

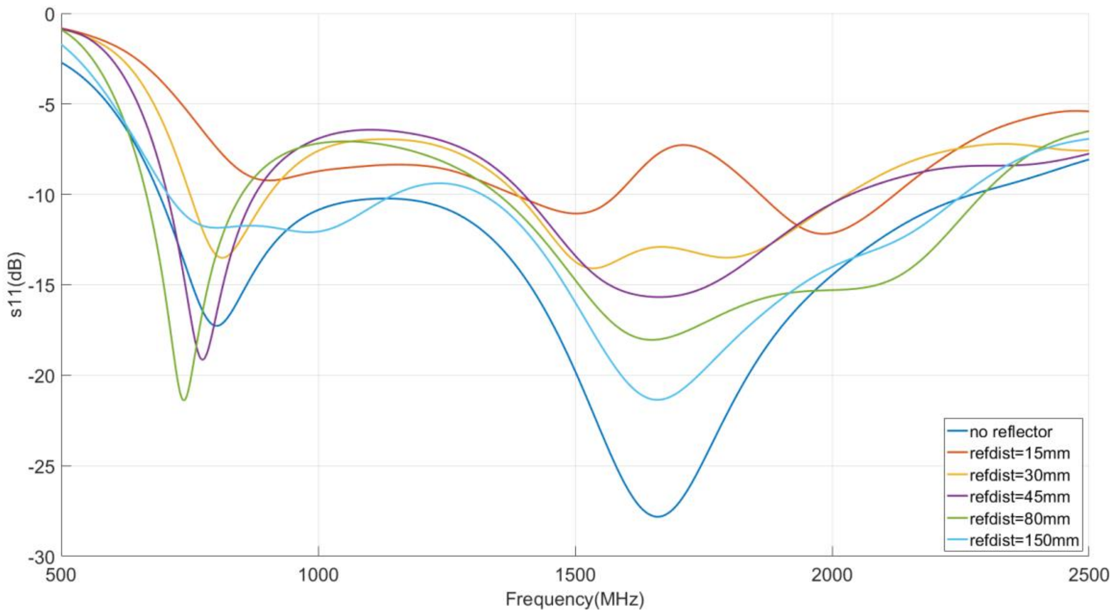

Figure 30. Effect of reflector distance on s_{11} performance

Since reflectors cannot be implemented without making the system bulky, frequency selective surfaces (FSS) can be used to miniaturize the antenna. FSS can be tuned as a reflector, director or absorber for specific use and adds flexibility to antenna design. It is a periodic arrangement of unit cells. The main advantage of FSS compared to traditional PEC is that, FSS can be placed closer to the antenna without affecting the input impedance.

An FSS unit cell reflecting the frequency band of interest and acting transparent to other frequencies is chosen from Alqadami's antenna design with an FSS [12][12]. In his work, Alqadami reported that proposed FSS is suitable for 1-2.5GHz frequency band. Figure 31 shows the FSS unit cell proposed in [12] and its simulation setup. Proposed unit cell consists of a square patch with four extended open-ended U-slots. The patch is connected to a 3-segments meander line from each corner. It is designed on one side of a 1.5mm thick FR-4 substrate.

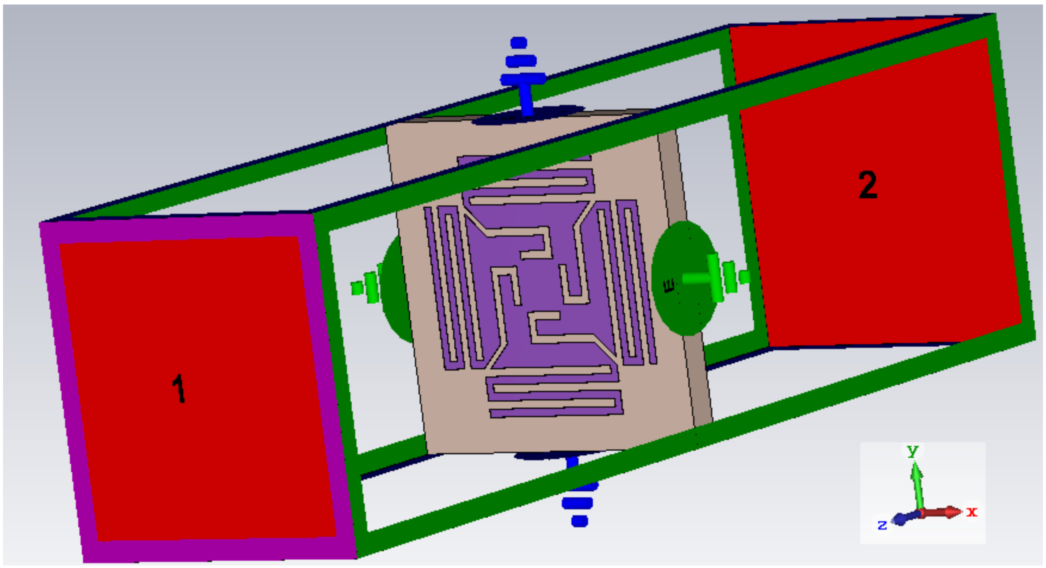

Figure 31. FSS unit cell model and simulation setup

To model the periodic nature of the FSS illuminated by an plane wave, unit cell is simulated with PEC and perfect magnetic conductor (PMC) walls in x and y directions, respectively. The choice of PEC or PMC walls can be explained based on the image theory. According to the image theory, image of a vertically oriented electric source over a PEC and image of a horizontally oriented electric source over a PMC are in the same direction with the actual source. Since incident wave is normal to PEC walls and tangential to PMC walls, PEC walls will create x-polarized images along x direction, and PMC walls will create x-polarized images along y direction. Note that, this kind of a simulation model is applicable only to simulate normal incidence excitation. If oblique incidence needs to be simulated, periodic boundary conditions should be used instead of PEC and PMC walls. Figure 32 shows s21 and s11 results of the FSS structure. The unit cell acts as a reflector for 1.1-1.8 GHz band while acting transparent to other frequencies. Another figure of merit for FSS performance is the reflection phase. Useful bandwidth is defined as frequencies where phase of reflected wave is between $\mp 90°$ so that phase is not inverted. Figure 33 shows reflection phase of the FSS unit cell. FSS exhibit decent reflection phase in 0.7-2.3GHz band. For this simulation, spacing between periodic structures is as small as 0.1mm.

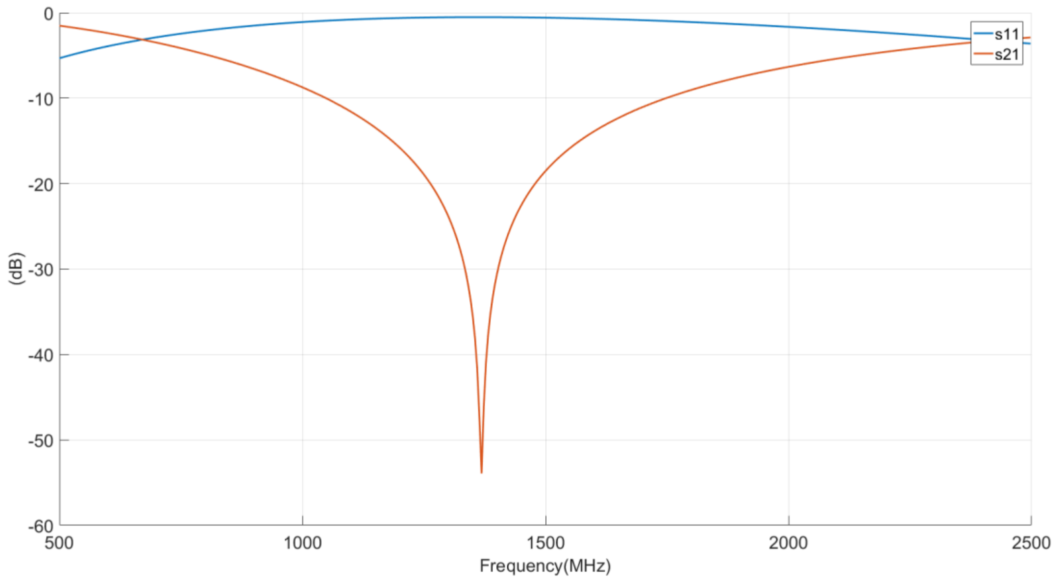

Figure 32. Reflection and Transmission performance of FSS unit cell

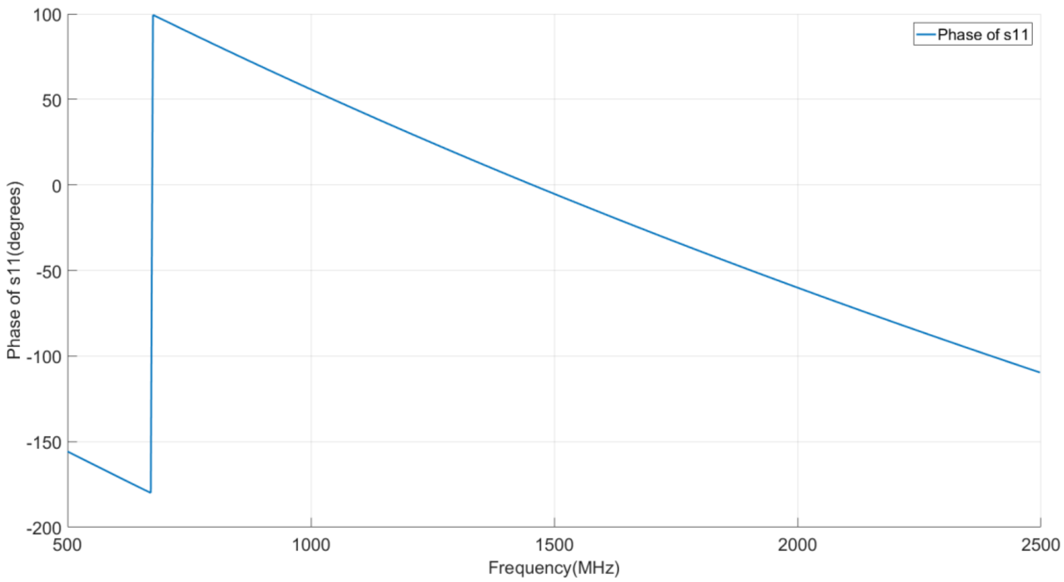

Figure 33. Reflection phase of FSS unit cell

FSS is simulated together with the antenna to observe its effects on the radiation pattern and input return loss performance of the antenna. When radiation patterns at different frequencies within the operational bandwidth are examined, it is observed that FSS behaves like a reflector for some frequencies but it behaves like a director for other frequencies. This is not a desired situation. Hence the distance between FSS and the antenna is varied to investigate whether same reflecting behavior can be obtained throughout the bandwidth for a specific spacing value. However satisfactory results could not be obtained. Then the periodicity of the FSS is varied to investigate its effects. During these analyses it is observed that when spacing between unit cells is increased, FSS behaves like a director for the whole operational bandwidth. The best performance is obtained when spacing between periodic structures is 3.4mm, which corresponds to a unit cell size of 16.2mmx16.2mm. Finally, the smallest spacing between the FSS and the antenna that does not disturb the return loss performance of the antenna is found to be 15mm.

After examination of infinite periodic array performance, a finite array of 49 (7x7) unit cells is assembled together. As shown in Figure 34, no space is left at the edges of the substrate used for FSS. Consequently, the size of FSS substrate (7x16.2mm-3.4mm=110mm) and the size of antenna substrate are same.

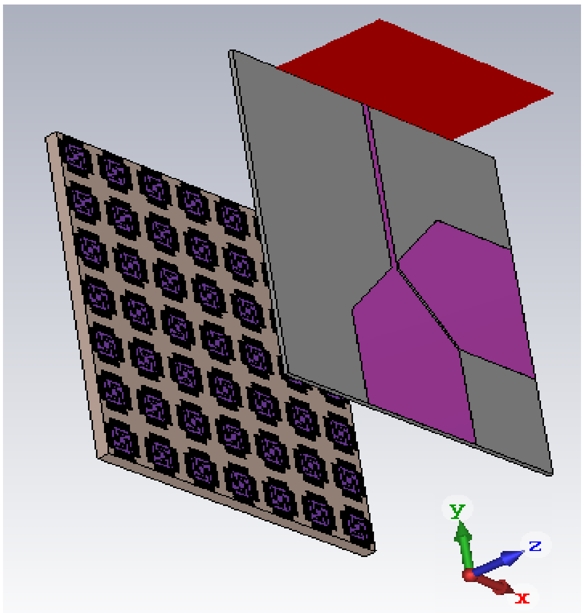

Figure 34. Antenna with FSS configuration

Input return loss of the antenna is presented in Figure 35 in comparison with the results obtained with PEC reflector. It can be observed that when PEC was disturbing the input return loss characteristic of the antenna at such a close spacing, the FSS structure does not have a significant effect on the input return loss behavior. However on the other hand, it should be noted that the FSS structure could not provide a uni-directional radiation characteristic as good as the PEC reflector.

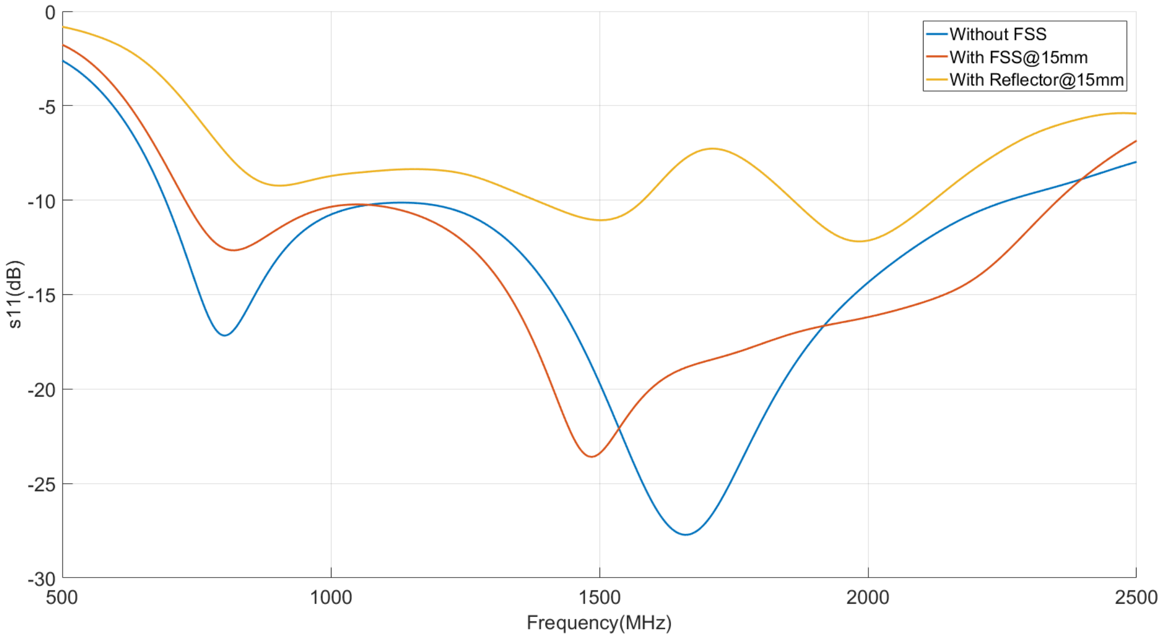

Figure 35. s_{11} performance of antenna with FSS

The effect of FSS on the radiation characteristics of the antenna is investigated. Since FSS will be utilized as a director, it will be placed between antenna and target area. Figure 36 shows E-plane radiation pattern of the antenna at 1GHz with FSS placed either behind (-z direction) or in front of (+z direction) the antenna. These radiation patterns shown that FSS behaves like a director because in both cases the radiation is enhanced in the direction that FSS is placed. It is also observed that 4dB of front to back ratio (FBR) is achieved when FSS is placed behind the antenna. Note that behind the antenna and in front of the antenna directions are defined by assuming that the feed line determines the front side of the antenna. As discussed before, this FBR is not as good as the FBR achieved by PEC reflector. Therefore, the trade-off between the minimum spacing between the reflector/director and antenna that does not affect the input return loss of the antenna and the FBR should be evaluated for a specific application. In this application low profile of the antenna is evaluated to be more important and FSS structure is chosen to improve radiation characteristics of the antenna.

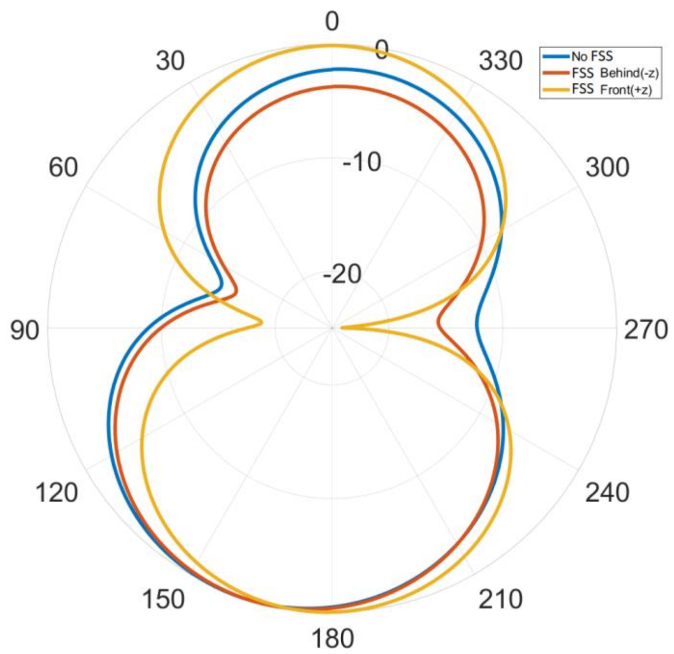

Figure 36. Radiation pattern of antenna with and without FSS @1GHz

Due to frequency dependent nature of FSS, FBR may change with frequency. Figure 37 shows radiation patterns at the center and end of the operating frequency band when FSS is placed either behind or in front of the antenna. Spacing between antenna and FSS is 1.5cm for all cases. It can be seen that at least 4 dB of front to back ratio is achieved for all frequencies and FBR increases as frequency gets larger.

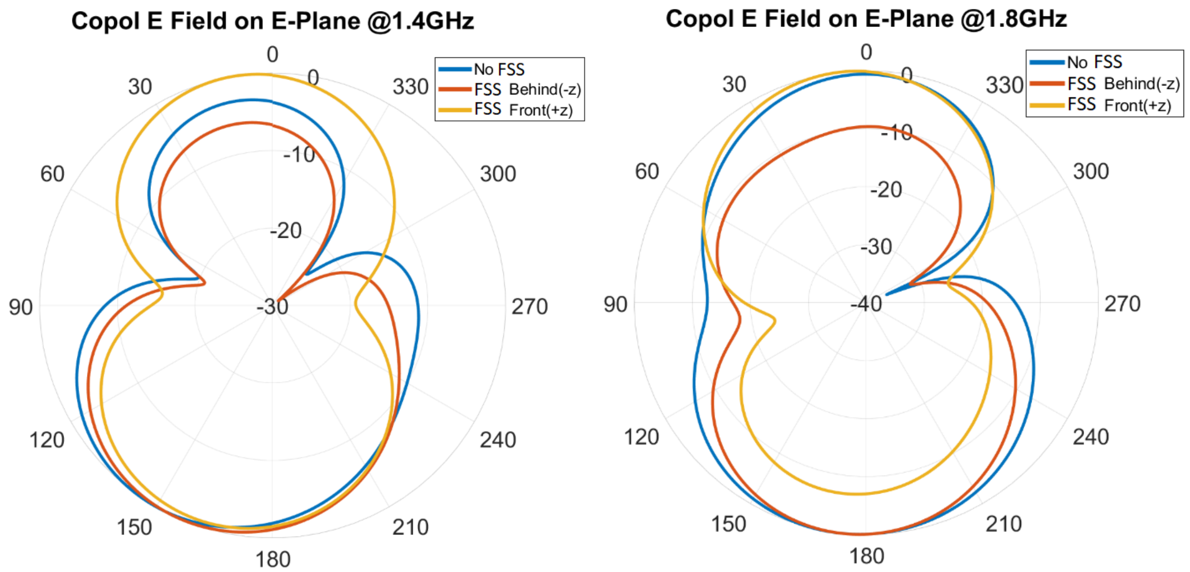

Figure 37. Co-pol E Field Radiation Patterns on E-Plane for various models and frequencies

2.5. Near Field Analysis with Head Phantom

In order to simulate the antenna performance for brain imaging systems more realistically, a human head phantom is introduced between two antennas. Figure 38 shows such simulation configuration and describes ports on both antennas. The head model used for this setup is “Hugo” from CST voxel family and all available tissues are included in the simulation. Antennas are placed next to head model with no space in between to smoothen sharp permittivity transition from air to head. Port 1 and port 3 are feeding the horizontally oriented dipoles and corresponding feedlines are on the back side (away from head) of the antenna while dipole arms serving as ground plane for these feedlines are on the front side (towards head) of the antenna. Port 2 and port 4 are feeding the vertically oriented dipoles and all dipole arm locations are on the opposite side of the substrate compared to horizontally oriented dipoles.

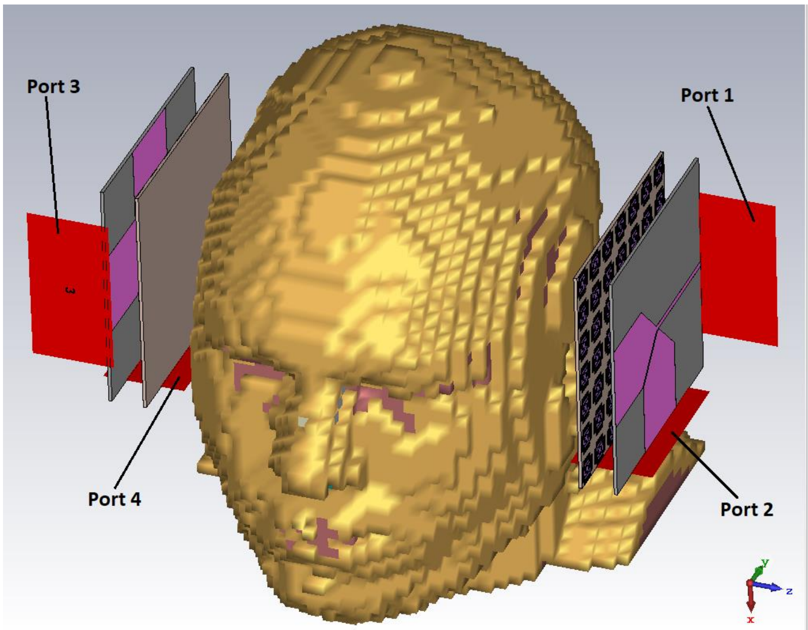

Figure 38. Simulation configuration with human head model

First, the effect of the presence of the head on antenna input return loss is investigated. Figure 39 shows the input return loss of the antenna with and without head. Although slight degradation due to reflections from the head is observed, the input return loss remained below -10dB throughout the bandwidth.

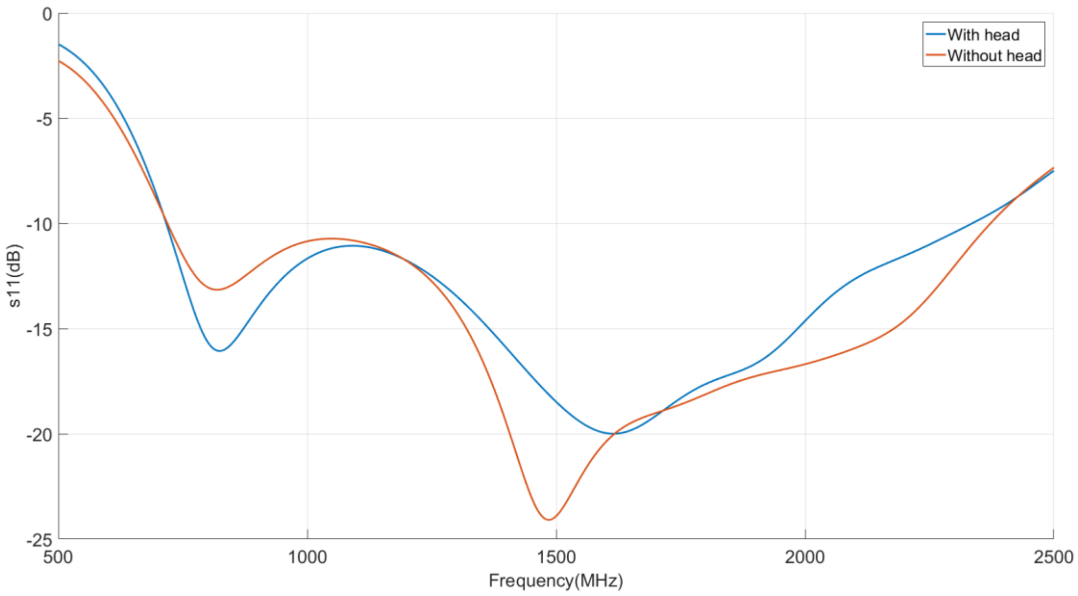

Figure 39. Effect of introducing head model on s_{11} performance

In order to investigate the signal transfer between two antennas at opposite sides of the head 4 different scenarios are studied. In the first case antennas are placed without FSS in between head and the radiating element. Then s_{31} which is the interaction between horizontally oriented antennas is simulated in the absence and presence of the head model. Then same two situations are simulated when FSSs are placed between antennas and head. Figure 40 shows s_{31} comparison of these configurations.

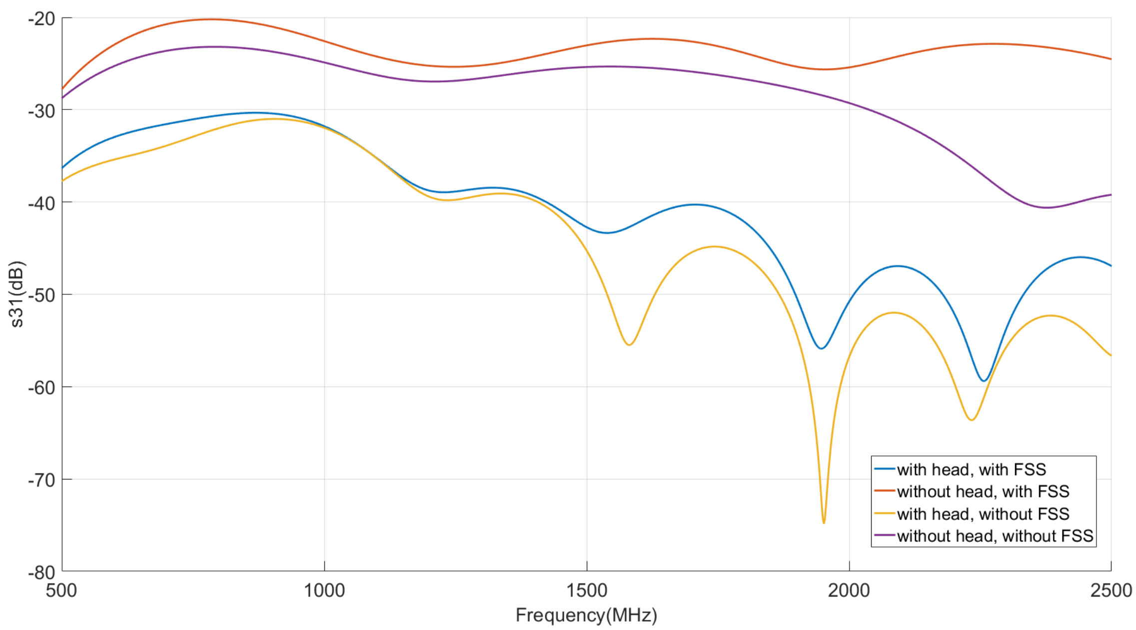

Figure 40. Interaction between horizontally oriented antennas for various configurations

Received signal level is higher when there is no head and antennas are in line of sight. This is an expected result since as the waves travel through the head, they are subject to a higher propagation loss and reflection. Received signal level is higher when frequency selective surface(FSS) is present. This confirms the mentioned directive behavior of FSS. Similar results are obtained for s_{42} which is the interaction between vertically oriented antennas on both sides of the head. Figure 41 shows s_{42} comparison between various configurations.

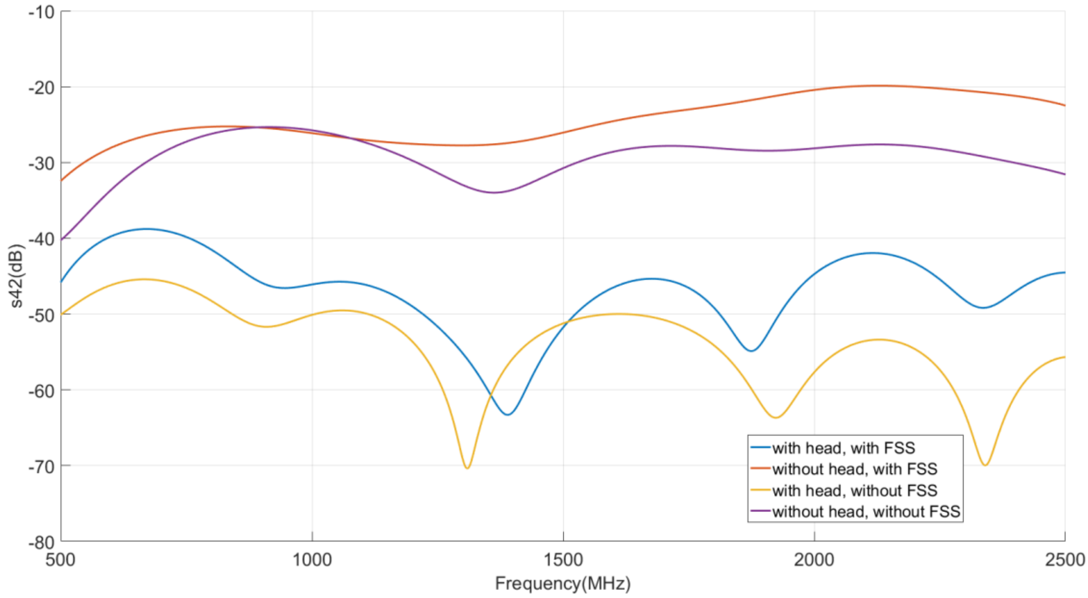

Figure 41. Interaction between vertically oriented antennas for various configurations

To compare the received signal levels for horizontal (HP) and vertical (VP) polarizations, corresponding s-parameters are presented in Figure 42 when there isn't any head model between antennas. Within the frequency band of interest, generally the received signal is slightly higher for horizontal polarization. This difference is due to the relative positions of antennas and FSS. Recall from Section 2.4 that the FBR is better when the FSS is placed behind the antenna. From Figure 38 it can be seen that the FSS is behind the antenna for horizontal polarization and in front of the antenna for vertical polarization. Consequently, signal level is higher for HP.

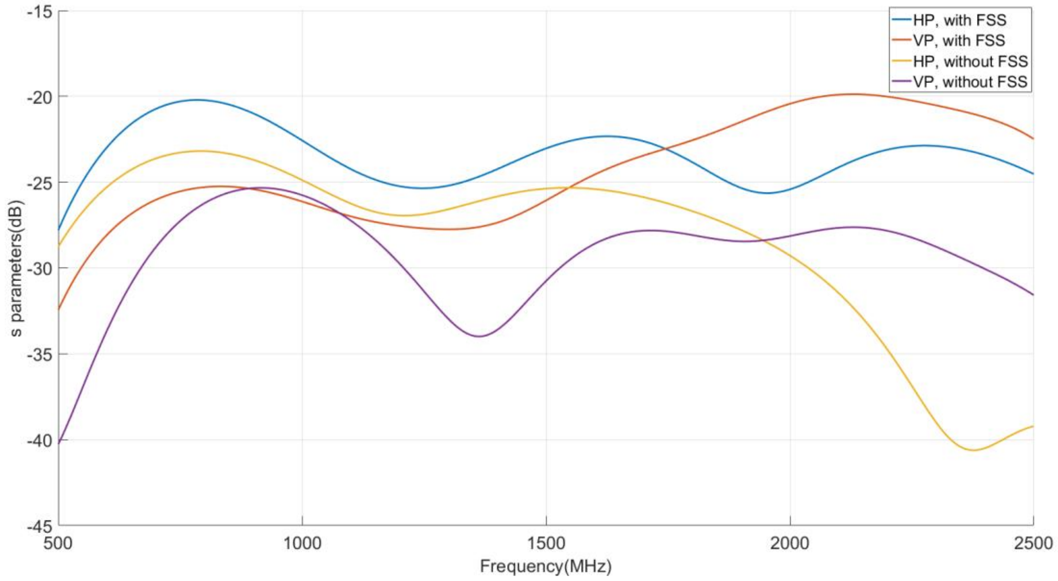

Figure 42. Interaction between antennas without head model for various configurations

The received signals for two different polarizations in the presence of the head model are presented in Figure 43. When there is head model, the received signal is higher for HP as well due to the reason discussed above. The interesting observation about this configuration is that, the nulls and peaks of the received signal occurs at different frequencies for different polarizations which implies that polarization diversity provides more data for a better image reconstruction.

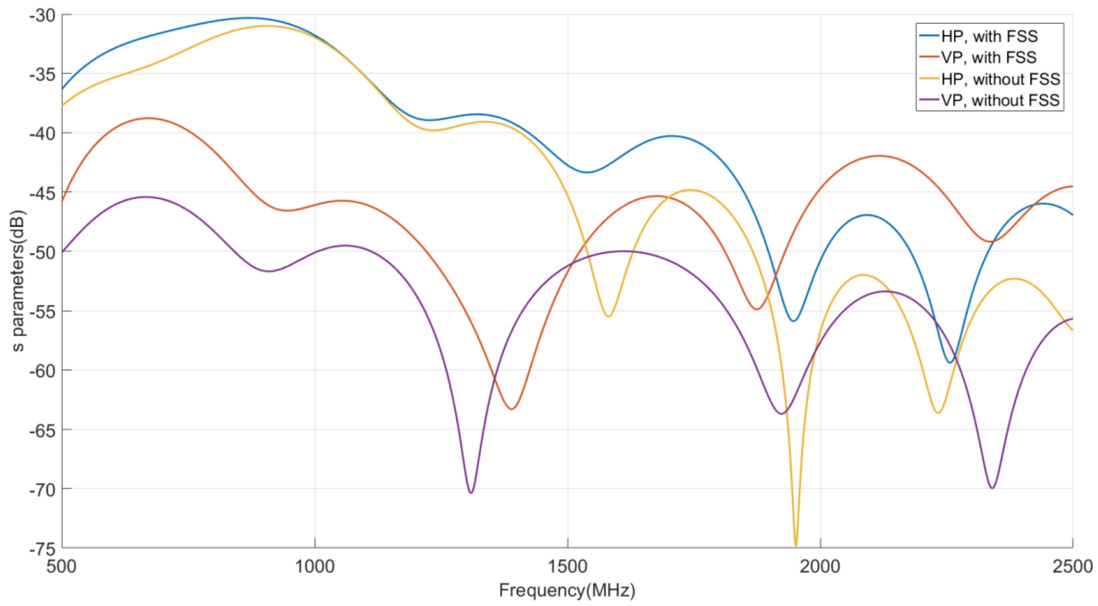

Figure 43. Interaction between antennas with head model for various configurations

The coupling between antennas on the same substrate are also studied for different configurations mentioned above and results are presented in Figure 44. It can be observed that the isolation between the antennas is better that 20dB when there isn't FSS structure and it is better that 19dB when there is FSS. When head model is introduced, the coupling between the antennas increases as expected due to reflections and scattering from head.

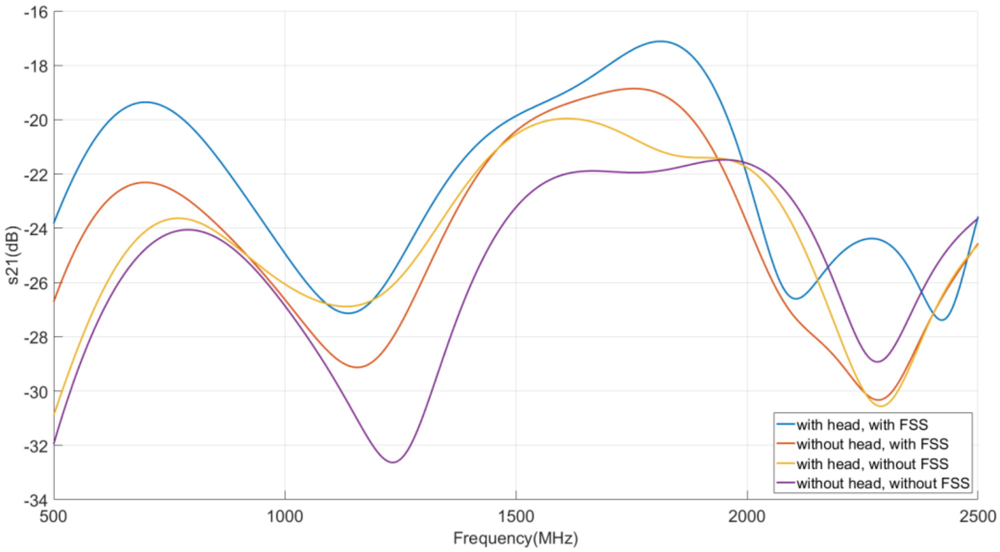

Figure 44. Coupling between antennas on the same substrate for various configurations

So far in this section, interactions between antenna ports are examined. Although scattering parameters might seem reasonable when head is present between antennas, waves might be reflected from head due to sharp permittivity change at air to head interface. One way to ensure that waves are able to penetrate through head is to examine electric field distribution in head for configurations mentioned above. Figure 45 shows electric field distribution for various in-band frequencies when horizontally oriented antenna is excited. It is clear that there are no sharp changes at the air-head interface in terms of field intensity. Note that although field intensity decreases towards the far side of the head, when the overall MIMO array is employed, those areas will be illuminated by other antennas placed closer to them. Such examination on electric field distribution is done in literature where successful image reconstruction is carried out with similar field distribution [21].

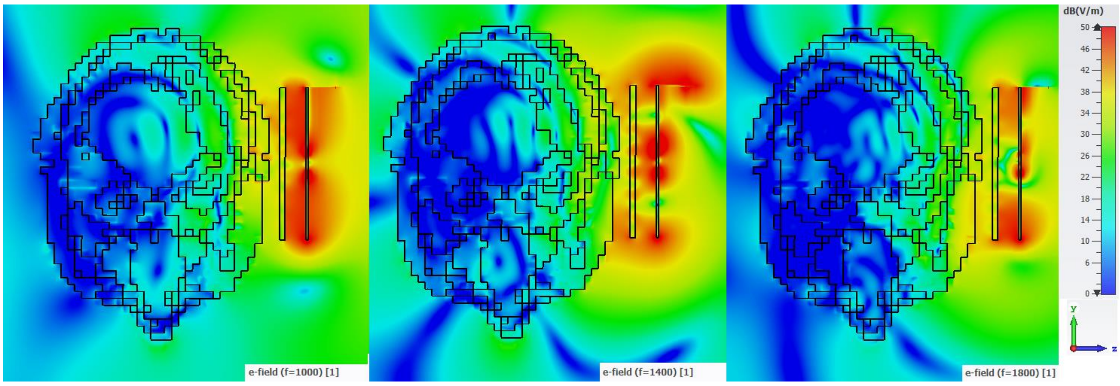

Figure 45. Electric field distribution at 1GHz, 1.4GHz, 1.8GHz

Figure 46 shows electric field distribution with and without FSS present between head and antenna. Although field intensity in the brain is similar in both cases, field intensity decreases slightly more when FSS is not used, suggesting FSS smoothens air-head interface. As a result, FSS can be used as a matching layer to improve penetration through the head.

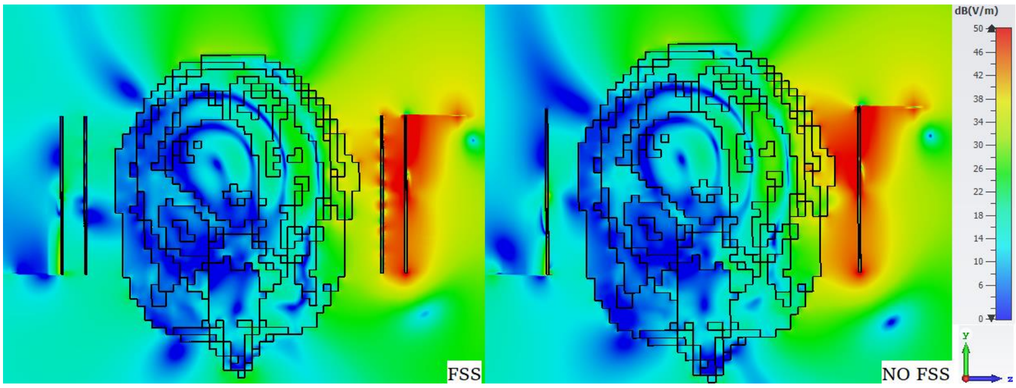

Figure 46. Electric field distribution with FSS and without FSS

CHAPTER III

Measurement Results

3.1. Realized Antenna

In order to support the simulation results in a practical manner, proposed antenna is realized, measured and results are compared with simulation results. Top view of the realized antenna can be seen in Figure 47.

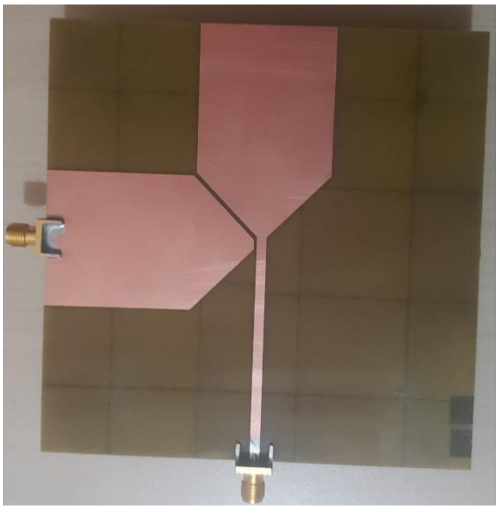

Figure 47. Top view of the realized antenna

After designing antenna on CST Studio Suite 2019 and determining final dimensions, gerber files of radiating element and FSS are generated on Mentor Graphics Pads Professional software. Using these layout files, antenna elements are manufactured by LPKF ProtoMat S100 circuit board printer on a 1.5mm thick FR-4 substrate with 18μm copper thickness. 3 sets of 4 foam supporting columns of 1.5cm, 2cm and 2.5cm are used to suspend the radiating element over FSS at different spacings. Top view of manufactured FSS can be seen in Figure 48.

Figure 48. Top view of realized frequency selective surface

2 SMA connectors are added to the microstrip feedlines connecting to an arm of each dipole. While center pins are soldered to feedlines, ground pins are soldered to related dipole's other arm serving as ground plane for the feedline. Such configuration can be seen in Figure 49.

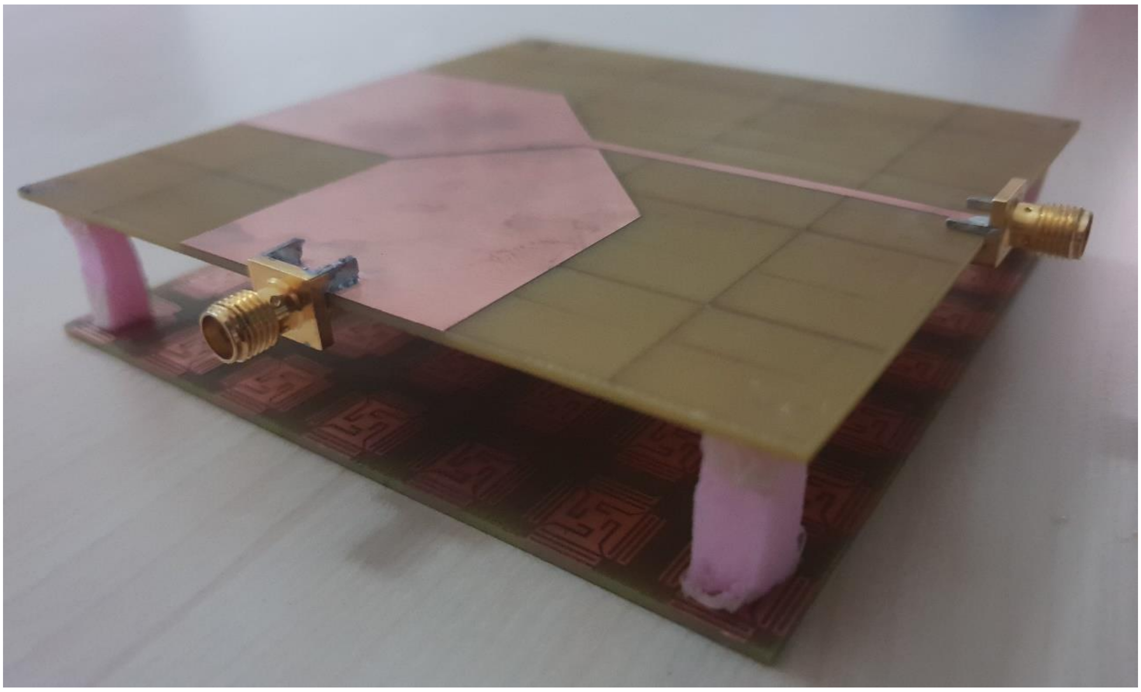

Figure 49. Manufactured antenna and FSS

3.2. Antenna Measurements

Agilent 5071c network analyzer is used to measure s_{11} performance of the antenna. 1-port calibration is done to compensate the coaxial cable used between the antenna and the network analyzer. Measurement is done in an open space to minimize the inaccuracies caused by reflections. Figure 50 shows the comparison between simulated and measured s_{11} results.

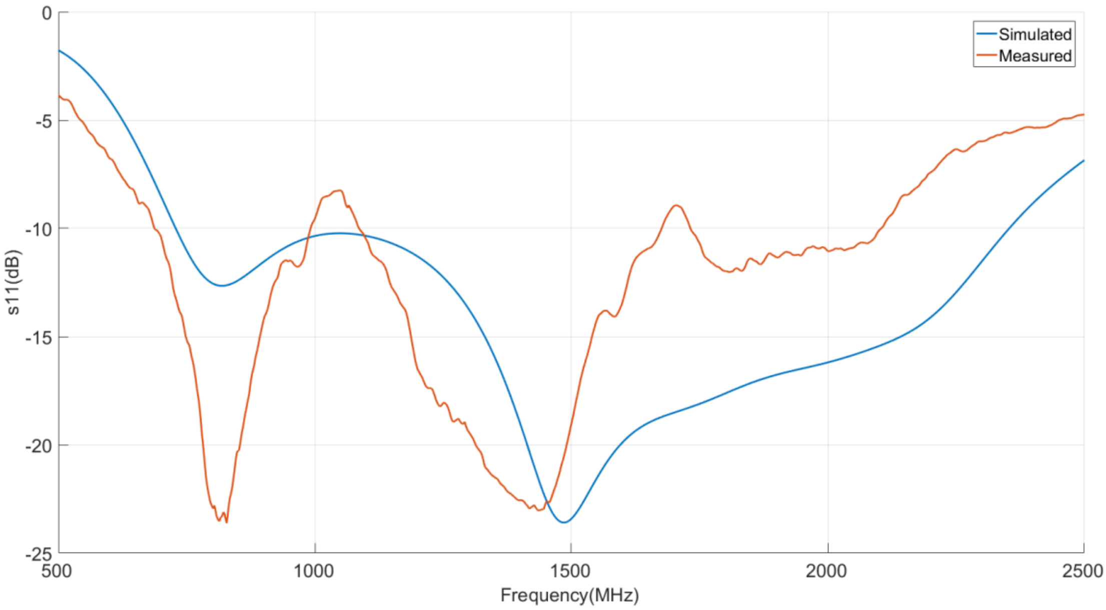

Figure 50. Simulated vs measured s_{11} results

It is clear that there is some difference in terms of frequencies of resonance and distance between these frequencies, as well as matching level of these resonances. In simulation, the antenna is excited by an ideal wave port. However, practically the antenna is excited using a SMA connector. Also, when measuring the antenna, plastic mechanism used to suspend the antenna and coaxial cables are very close to antenna and slightly affects the antenna performance. Despite such differences, measured results show that desired minimum operating frequency of 900 MHz is achieved. Also, realized antenna is usable up to 2.1GHz, ensuring optimum penetration range to detect all layers of the brain.

In order to ensure isolation between two ports of the antenna, s_{21} measurement is also carried out. 2-port calibration is done to compensate coaxial cables and tracking errors between network analyzer ports. Figure 51 shows comparison of simulated and measured isolation between dipole pair on the same substrate. Although measured results do not exhibit frequency dependent characteristics as simulated results do, isolation values are close to each other.

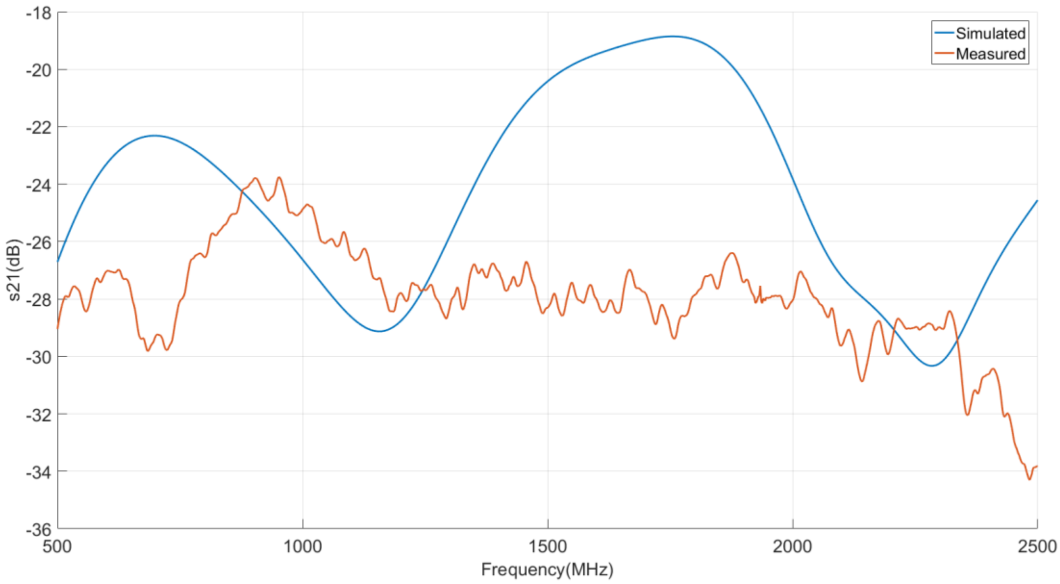

Figure 51. Simulated vs measured s_{21} results

Radiation pattern measurements of the realized antenna are also carried out. For this measurement anechoic chamber within Ayaslı Research Center of Electrical and Electronic Engineering Department of METU is utilized. Figure 52 shows the anechoic chamber and measurement setup.

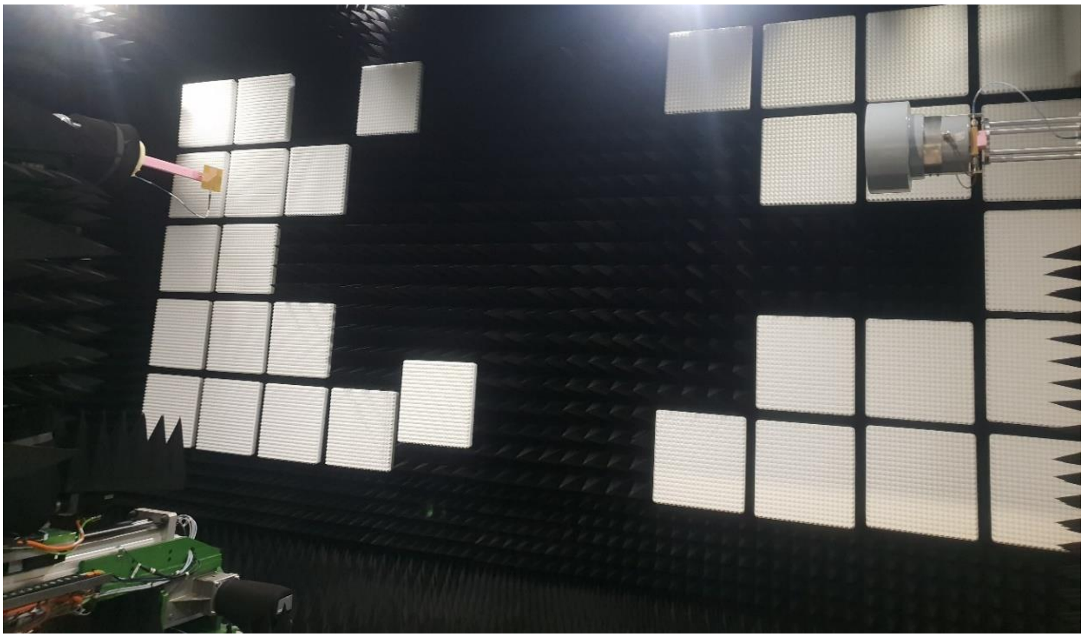

Figure 52. Anechoic chamber and measurement setup

Figure 53 shows comparison between simulated and measured results of co-polarized radiation patterns in E-plane for various frequencies. Although lobe shapes and null levels are different for some frequencies, front to back ratios are similar. Slight difference between left and right nulls might be associated with the effect of SMA connector at the end of one of the dipole arms which is a conductor in very close proximity of the antenna. Results with FSS are very similar for changing FSS distance in terms of both lobe shapes and front to back ratios. Although front to back ratios are low for some frequencies, directive effect of FSS can be seen with front to back ratios as high as 7dB especially for higher frequencies in operating frequency band. Cross-polarized radiation patterns are also measured and compared to simulation results in Figure 54 when there isn't any FSS layer. Increasing cross-pol levels with frequency seen in simulation results are not observed in measurements. In fact, cross-pol levels decrease with increasing frequency. This may be due to low signal level of cross-pol components. The accuracy of cross-pol measurements is limited by the dynamic range of the measurement set-up. Nevertheless, measured cross-pol levels are at least 30 dB below co-polar components. Figure 55 shows comparison of measured and simulated co-pol radiation patterns in H-plane. Although there is up to 6 dB difference from maximum radiation magnitude for some directions in 1.8GHz, antenna exhibits nearly omnidirectional pattern for all frequencies in operating frequency band. Also, simulated and measured results are very similar for all frequencies.

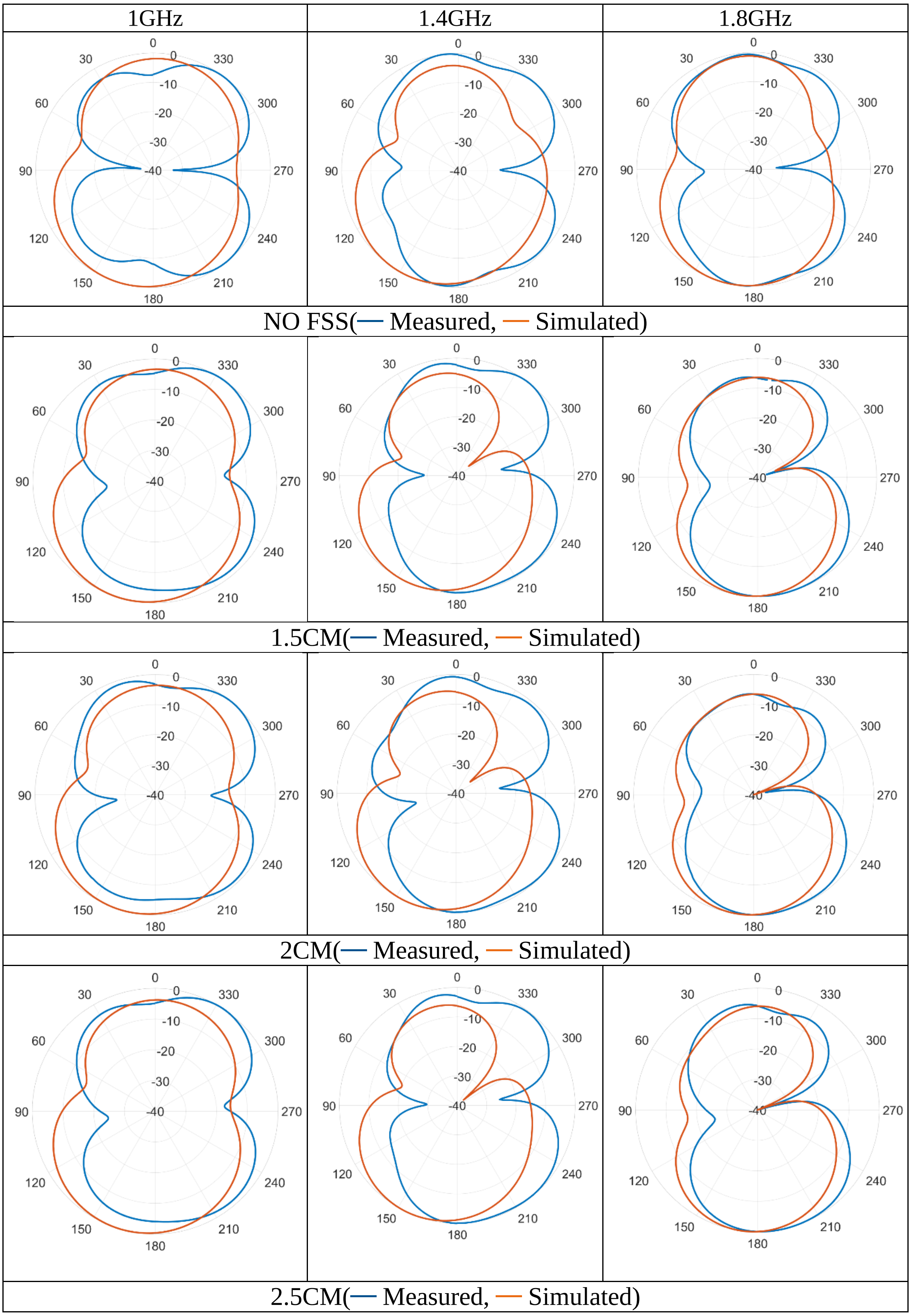

Figure 53. Measured vs simulated co-pol radiation patterns in E-plane for various FSS distances and frequencies

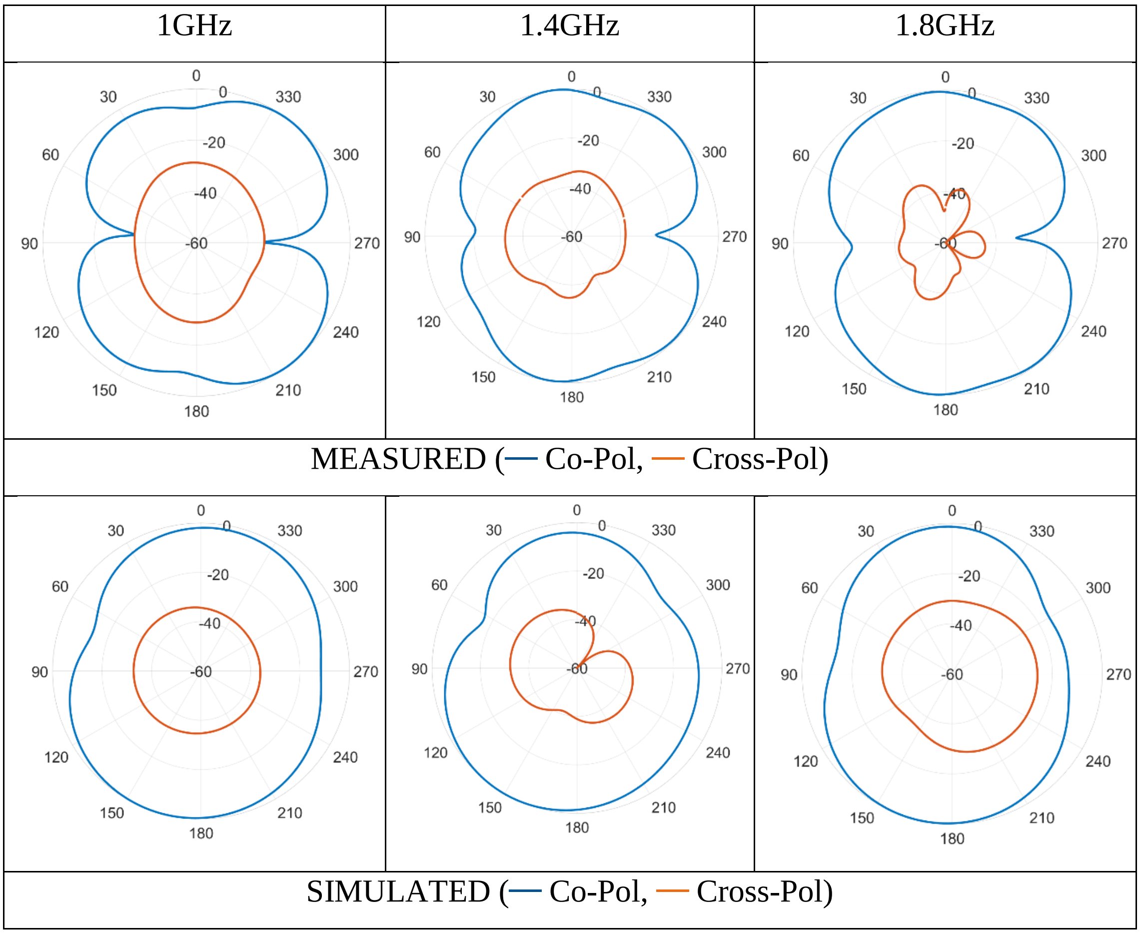

Figure 54. Measured vs simulated co-pol and crosspol radiation patterns in E-plane for various frequencies

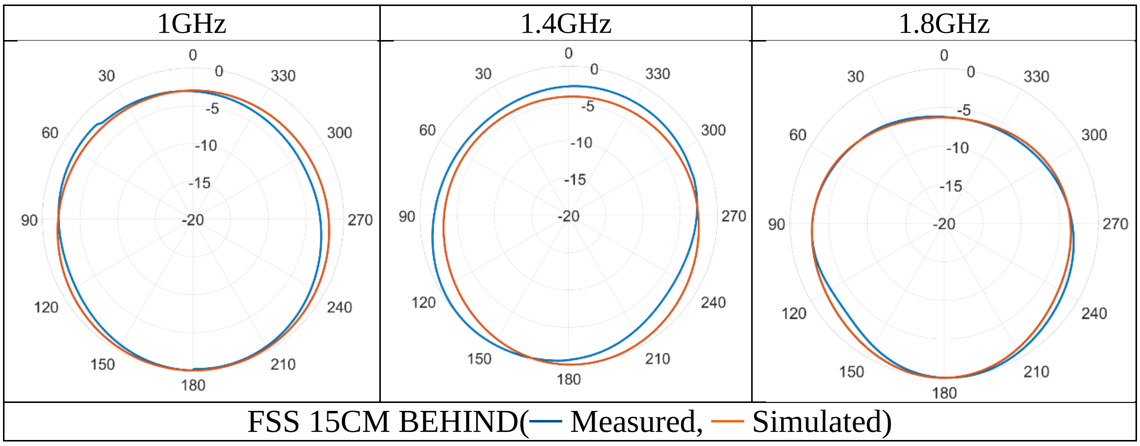

Figure 55. Measured vs simulated co-pol radiation patterns in H-plane for various frequencies

CHAPTER IV

Conclusion and Future Work

4.1. Conclusion

In this thesis, a low profile, low cost, wide band, dual polarized antipodal printed dipole antenna for brain imaging is proposed. Novelty of the antenna proposed in this thesis over numerous antennas proposed for microwave brain imaging is adding dual polarization feature while maintaining other requirements for microwave brain imaging. In literature there is another dual polarized antenna intended for microwave imaging that is optimized for 3.1-9.6 GHz band [23]. Such an antenna cannot be used for brain imaging since the frequency band is not appropriate for penetration into the brain. Lowering minimum operating frequency down to 900 MHz so that radiated field is able to penetrate all layers of the brain has been one of the main challenges of this work. Dual polarization requires two dipoles instead of one and therefore, dual polarized antennas are inherently larger than a single polarized antenna. Although proposed antenna is smaller than half-wavelength dipole, further miniaturization is required to meet the portable system requirement. When compared to other antennas for microwave brain imaging, 11x11x1.8cm dimensions stand out as large and such dimensions limits the number of antennas in MIMO system. Further miniaturization on the proposed antenna have been attempted. However, such optimizations are observed to degrade antenna performance inevitably.

Dual polarization performance parameters such as isolation between ports and cross-pol radiation are satisfactory for the proposed antenna to be practically used in microwave imaging of brain. Over 19 dB isolation between ports on the same substrate as well as more than 20dB cross-polarization suppression is achieved throughout the bandwidth, suggesting appropriate separation of data obtained from dipole pairs.

Detailed parametric optimizations of antenna parameters are carried out during this thesis. Rather than parametric optimization for best performance only, systematic examination of effects of each antenna parameter on the antenna properties is also carried out. Therefore, this thesis serves as a general guide for designing similar antennas.

In the final design, FSS is as close as 15 mm to the radiating element which is much more practical compared to a PEC placed 150mm behind the antenna not the affect the input return loss characteristics of the antenna. With FSS, 4dB front to back ratio is achieved throughout the bandwidth according to simulation results. Despite FSS being a useful addition to the system for radiation pattern improvement, performance of the whole antenna is affected by FSS's own performance. Although simulation results showed at least 4 dB of front to back ratio, measurement results show front to back ratios as low as 2dB. This undesirable result is mostly due to narrowband property of the used FSS unit cell. An FSS with wider frequency band can be used to improve radiation performance of the antenna on whole band. Since unit cell dimensions of FSS are much smaller compared to dipole, FSS is more susceptible to inaccuracies in manufacturing. In order for the proposed antenna to be used in practical applications in a more reliable manner, a frequency selective surface with wider bandwidth must be chosen and preferably manufactured in an etching machine with higher accuracy.

Another useful result obtained by examining electric field distribution in the brain when illuminated by the proposed antenna is that waves are able to penetrate through the brain and no matching layer is required. Using matching layer between the head and antennas is common in literature and increases cost as well as complexity of the system. There are even examples of microwave imaging systems where organ to be imaged is afloat inside a tank filled with matching liquid to reduce reflections.

4.2. Future Work

As mentioned in previous chapters, there are many trade-offs to be analyzed in antenna design for microwave imaging, mostly parallel to properties of the final system. Further optimization can be done according to these properties. For example, in this work, FR-4 material is used as the antenna substrate. Since FR-4 is a very common material, cost of the antenna is minimal. Substrates with advanced properties can be used to introduce new features to the system. Figure 56 shows antenna with poly-di-methyl-siloxane (PDMS) substrate which is a flexible material. Such a feature requires further optimization, increases complexity and cost however can be useful for mobility since a flexible substrate is more durable and break-resistant, hence more desirable for wearable antenna technology.

Figure 56. Flexible antenna with PDMS substrate

The proposed antenna is based on a printed dipole antenna. Since dipole antennas are one of the most basic and common antennas, design limitations such as dimensions are well defined. Instead of integrating dipole antennas to obtain dual polarization, other antenna types which can be optimized to be smaller in size can be investigated. There are examples in literature where each component of polarization is obtained by a different antenna type.

Imaging quality of a microwave imaging system heavily depends on the antenna performance. Therefore, it is reasonable to start with designing the antenna and define specifications and limits for the system. Then, other elements such as switching circuitry, transceiver or image reconstruction algorithm can be designed. Although designing a microwave imaging system is a multi-disciplinary project, every system component is related to each other. Therefore, it is a good idea for one to be involved in other parts of the project.

References

[1]S. Ahdi Rezaeieh, A. Zamani and A. M. Abbosh, "3-D Wideband Antenna for Head-Imaging System with Performance Verification in Brain Tumor Detection," *IEEE Antennas and Wireless Propagation Letters*, vol. 14, pp. 910-914, 2015.

[2]K. S. Sultan, B. Mohammed, M. Manoufali and A. M. Abbosh, "Portable Electromagnetic Knee Imaging System," *IEEE Transactions on Antennas and Propagation*, vol. 69, no. 10, pp. 6824-6837, Oct. 2021.

[3]I. Saied and T. Arslan, "Microwave Imaging Algorithm for Detecting Brain Disorders," 2019 29th International Conference Radioelektronika, pp. 1-5, 2019.

[4]Y. -S. Cho, H. -K. Jung, C. Cheon and Y. -S. Chung, "Adaptive Back-Projection Algorithm Based on Climb Method for Microwave Imaging," *IEEE Transactions on Magnetics*, vol. 52, no. 3, pp. 1-4, March 2016.

[5]A. Brankovic, "Unsupervised Algorithm for Brain Anomalies Localization in Electromagnetic Imaging," in *IEEE Transactions on Computational Imaging*, vol. 6, pp. 1595-1606, 2020.

[6]I. Bisio, "Variable-Exponent Lebesgue-Space Inversion for Brain Stroke Microwave Imaging," in *IEEE Transactions on Microwave Theory and Techniques*, vol. 68, no. 5, pp. 1882-1895, May 2020.

[7]P. Tournier, M. Bonazzoli, "Numerical Modeling and High-Speed Parallel Computing: New Perspectives on Tomographic Microwave Imaging for Brain Stroke Detection and Monitoring.," in *IEEE Antennas and Propagation Magazine*, vol. 59, no. 5, pp. 98-110, Oct. 2017.

[8]M. Rokunuzzaman, M. Samsuzzaman, "Unidirectional Wideband 3-D Antenna for Human Head-Imaging Application," in *IEEE Antennas and Wireless Propagation Letters*, vol. 16, pp. 169-172, 2017.

[9]M. Rokunuzzaman, A. Ahmed, T. C. Baum, "Compact 3-D Antenna for Medical Diagnosis of the Human Head," in *IEEE Transactions on Antennas and Propagation*, vol. 67, no. 8, pp. 5093-5103, Aug. 2019.

[10]A. Afyf and L. Bellarbi, "A novel miniaturized UWB antenna for microwave imaging," 2014 International Conference on Multimedia Computing and Systems (ICMCS), pp. 1475-1478, 2014.

[11]M. A. Al-Joumayly, S. M. Aguilar, N. Behdad and S. C. Hagness, "Dual-Band Miniaturized Patch Antennas for Microwave Breast Imaging," *IEEE Antennas and Wireless Propagation Letters*, vol. 9, pp. 268-271, 2010.

[12]A. S. M. Alqadami, K. S. Bialkowski, "Wearable Electromagnetic Head Imaging System Using Flexible Wideband Antenna Array Based on Polymer Technology for Brain Stroke Diagnosis," *IEEE Transactions on Biomedical Circuits and Systems,* vol. 13, no. 1, pp. 124-134, Feb. 2019.

[13] S. M. Michaelson, "Human exposure to nonionizing radiant energy—Potential hazards and safety standards," *Proceedings of the IEEE*, vol. 60, no. 4, pp. 389-421, April 1972.

[14] C. C. Johnson and A. W. Guy, "Nonionizing electromagnetic wave effects in biological materials and systems," Proceedings of the IEEE, vol. 60, no. 6, pp. 692-718, June 1972.

[15]A. M. Abbosh, M. E. Bialkowski and W. C. Khor, "Design of an UWB Planar Monopole Antenna for Use in a Circular Cylindrical Microwave Imaging System," 2006 International Conference on Microwaves, Radar & Wireless Communications, pp. 947-950, 2006.

[16]Q. Fang, "Computational Methods for Microwave Medical Imaging", PhD Thesis, Thayer School of Engineering Dartmouth College, New Hampshire, USA, 2004

[17]I. Yamaura, "Measurements of 1.8 - 2.7-GHz Microwave Attenuation in the Human Torso," IEEE Transactions on Microwave Theory and Techniques, vol. 25, no. 8, pp. 707-710, Aug. 1977.

[18]N. Joachimowicz, C. Pichot and J. P. Hugonin, "Inverse scattering: an iterative numerical method for electromagnetic imaging," in IEEE Transactions on Antennas and Propagation, vol. 39, no. 12, pp. 1742-1753, Dec. 1991.

[19]A. T. Mobashsher, and A. Abbosh, “Three-dimensional folded antenna with ultra-wideband performance, directional radiation and compact size,” IET Microw, Antennas Propag., 2013.

[20]A. T. Mobashsher, and A. Abbosh, “Development of compact directional antenna utilising plane of symmetry for wideband brain stroke detection systems”, *Electronics Letters*, vol. 50. pp. 850-851, Aug. 2014.

[21]C. Deng, Y. Li, Z. Zhang and Z. Feng, "A Wideband High-Isolated Dual-Polarized Patch Antenna Using Two Different Balun Feedings," *IEEE Antennas and Wireless Propagation Letters*, vol. 13, pp. 1617-1619, 2014.

[22]A. T. Mobashsher, A. M. Abbosh, “On-site Rapid Diagnosis of Intracranial Hematoma using Portable Multi-Slice Microwave Imaging System,” Scientific Reports, vol. 6, no. 1, Nov. 2016.

[23]A. Sharma, G. Kumar and R. Kumar, "Design of Dual Polarized Ultra-Wideband Antenna for Microwave Imaging," 2018 International Conference on Intelligent Circuits and Systems (ICICS), 2018, pp. 121-125.

[24]D. Yang, H. Zeng, Y. Wen, “Design of Wideband Dual-Polarized Planar Antenna Using Multimode Concept”, International Journal of Antennas and Propagation, 2016.

[25]A. T. Mobashsher, A. M. Abbosh, Y. Wang, "Microwave System to Detect Traumatic Brain Injuries Using Compact Unidirectional Antenna and Wideband Transceiver with Verification on Realistic Head Phantom," in *IEEE Transactions on Microwave Theory and Techniques*, vol. 62, no. 9, pp. 1826-1836, Sept. 2014.

[26]N. Iqbal, S. Karamzadeh, “UWB Microstrip Antenna Design for Microwave Imaging Systems”, International Journal of Electronics, Mechanical and Mechatronics Engineering, pp. 7, 1411-1417, 2017.